Growth of Cloud Droplets in a Turbulent Environment

Wojciech W. Grabowski[1] and Lian-Ping Wang[2]

[1]Mesoscale and Microscale Meteorology Division, National Center for Atmospheric Research, Boulder, Colorado 80307; email: grabow@ucar.edu

[2]Department of Mechanical Engineering, University of Delaware, Newark, Delaware 19716; email: lwang@udel.edu

Annu. Rev. Fluid Mech. 2013. 45:293–324

First published online as a Review in Advance on October 5, 2012

The *Annual Review of Fluid Mechanics* is online at fluid.annualreviews.org

This article's doi: 10.1146/annurev-fluid-011212-140750

Keywords

condensational growth, turbulent collision-coalescence, particle-laden flow, cloud microphysical processes, weather, climate

Abstract

Motivated by the need to resolve the condensation-coalescence bottleneck in warm rain formation, a significant number of studies have emerged in the past 15 years concerning the growth of cloud droplets by water-vapor diffusion and by collision-coalescence in a turbulent environment. With regard to condensation, recent studies suggest that small-scale turbulence alone does not produce a significant broadening of the cloud-droplet spectrum because of the smearing of droplet-scale fluctuations by rapid turbulent and gravitational mixing. However, different diffusional-growth histories associated with large-eddy hopping could lead to a significant spectral broadening. In contrast, small-scale turbulence in cumulus clouds makes a significant contribution to the collision-coalescence of droplets, enhancing the collection kernel up to a factor of 5, especially for droplet pairs with a low gravitational collision rate. This moderate level of enhancement has a significant impact on warm rain initiation. The multiscale nature of turbulent cloud microphysical processes and open research issues are delineated throughout.

1. INTRODUCTION

Drizzle: light rain precipitation consisting of water droplets smaller than 0.5 mm in diameter

Stratocumulus cloud: a low, lumpy-looking widespread cloud with dark and light shading

CCN: cloud condensation nuclei

Atmospheric clouds dominate the visual appearance of Earth when viewed from space. Whereas visible clouds may extend over distances up to hundreds of kilometers, individual water droplets are typically only 5–20 μm in radius. In warm (i.e., above-freezing) clouds, droplets can further grow by collision-coalescence to form drizzle droplets or raindrops, a few hundred micrometers to several millimeters in diameter. Rainfall produced in such a way (referred to as warm rain, in contrast to precipitation formed by ice processes) accounts for approximately 30% of the total rainfall on the planet and roughly 70% of the total rain area in the tropics (Lau & Wu 2003).

Warm, shallow convective clouds, such as subtropical stratocumulus and tropical shallow cumulus, are critically important for Earth's climate and climate change. Because such clouds cover a large fraction of Earth's tropics and subtropics, they exert significant control over the partitioning of the incoming solar radiative flux into energy reflected back to space and energy absorbed by the climate system. At the same time, their impact on Earth's thermal radiation is small because the temperature of their tops is not much different than the temperature of the surface of the Earth. It follows that shallow clouds play a key role in climate change and climate sensitivity (e.g., Bony & Dufresne 2005), and their relatively small changes can offset the top-of-the-atmosphere radiative forcing due to anthropogenic carbon-dioxide emissions (e.g., Slingo 1990). Moreover, the size of droplets within these clouds affects the amount of solar radiation reflected back to space, whereas the removal of cloud water through precipitation processes can potentially affect such bulk cloud properties as the cloud fraction and cloud lifetime. These impacts are typically referred to as the first and second indirect aerosol effects, respectively (e.g., Twomey 1974, 1977; Albrecht 1989; Pincus & Baker 1994). The reference to aerosols in this context emphasizes the role of cloud condensation nuclei (CCN), small atmospheric aerosols involved in the formation of cloud droplets. Differences between the CCN in clean marine and polluted continental environments are primarily responsible for the observed differences between microphysical characteristics of clouds developing in these environments (Pruppacher & Klett 1997).

Numerical models applied to predict weather and study the climate cannot resolve all relevant scales, from the cloud microscale (subcentimeter) to the global scale (thousands of kilometers). In particular, the representation of cloud microphysical processes is often a source of significant uncertainty. For example, parameterizations of the autoconversion rate (i.e., the rate at which cloud water is converted into rain) could differ by a factor of 10 (Hsieh et al. 2009). The representation of shallow cumulus albedo in large-scale climate models is poor in comparison to satellite observations (Bender et al. 2006). Furthermore, when the horizontal grid length in these models is drastically varied (either because of the availability of high-performance computation or the need for a limited-area prediction), reliable parameterizations of cloud microphysical processes are required (Fiori et al. 2011).

This article reviews recent progress regarding the effects of cloud turbulence on the growth of cloud droplets and precipitation (rain) drops. Classical cloud physics textbooks (e.g., Rogers & Yau 1989, Pruppacher & Klett 1997) provide little insight on the role of cloud turbulence in the growth of cloud particles and the development of precipitation. Our goal is to fill this gap.

1.1. Droplet Activation and Growth: The Size-Gap Problem

The activation of CCN (e.g., near the cloud base where the humid air rises and its relative humidity crosses the saturation) is fairly accurately described by the theory developed by Koehler in the first quarter of the twentieth century (see Pruppacher & Klett 1997). This theory describes the equilibrium between humid air and a small water droplet with a dissolved CCN particle. It predicts

that the largest and most soluble CCN are activated first near the cloud base, and the activation of progressively smaller (and typically more numerous) CCN follows while the supersaturation continues to increase. Once a sufficient number of CCN are activated, the supersaturation begins to decrease (owing to the growth of the already activated droplets), and CCN activation is complete. Activated CCN are in the form of small solution droplets (typically with a radius around 1 μm) that further grow efficiently by the diffusion of water vapor (Beard & Ochs 1993, Raes 2006). During the diffusional growth, the rate at which the droplet radius increases is inversely proportional to the radius. This implies that a larger droplet grows (in radius) slower than a smaller one, and such a situation results in a narrow droplet-size spectrum if one considers only growth by diffusion.

In realistic cloud conditions, growth by water-vapor diffusion seldom produces droplets with radii close to 20 μm because of the low magnitude of the supersaturation field (see Section 3.1) and the time available for the growth ($\sim 10^3$ s). Gravitational collisions between cloud droplets, in which larger droplets grow by capturing smaller droplets by collision-coalescence, are effective when the droplet radius reaches approximately 40 μm (Pruppacher & Klett 1997). In general, it is difficult to explain the rapid growth of cloud droplets in the size range 15–40 μm in radius for which neither the diffusional mechanism nor the gravitational collision-coalescence mechanism is effective (i.e., the condensation-coalescence bottleneck or the size gap). The question is what drives droplet growth through this bottleneck size range. The onset of drizzle-size drops (~100 μm in radius) is still poorly understood, and this issue is regarded as an important unresolved problem in cloud physics. A related issue is the discrepancy between the width of observed and simulated size distributions of cloud droplets (Brenguier & Chaumat 2001).

Several mechanisms have been proposed to explain the rapid development of rain often observed in shallow convective clouds, including the entrainment of dry environmental air into the cloud, the effects of giant aerosol particles, turbulent fluctuations of the water-vapor supersaturation, and turbulent collision-coalescence. A review of these mechanisms and related early studies can be found in Beard & Ochs (1993).

Supersaturation: the relative degree of water-vapor pressure exceeding the saturation vapor pressure

Size gap: the size range of approximately 15–40 μm in which neither the diffusional growth nor gravitational collision is effective to increase the droplet size; also called the bottleneck size range

Cloud dynamics: mass, momentum, and energy transfer and transport within a cloud and between a cloud and its environment

Cloud microphysics: all processes by which cloud and precipitation particles form, grow, and transform

1.2. Scope: Impact of Turbulence on Cloud Microphysics

We focus on the effects of air turbulence on the growth of cloud droplets by the diffusion of water vapor and by collision-coalescence. When droplets are suspended in a turbulent cloud, they are transported and dispersed by large-scale energy-containing turbulent eddies of the order of 100 m. At the same time, they alter the local environment through mass (condensation and evaporation), momentum (viscous drag), and energy (latent heat) transfer at the scale of individual droplets. These local transfers can lead to noncontact and contact interactions between droplets and together can modulate the background airflow. For example, the phase transformation between water vapor in the air and the liquid water in the droplets, taking place at the droplet scale, introduces bulk buoyancy effects that drive cloud-scale motions. The extreme density contrast between the droplet and the air implies a significant (at the microscale) droplet inertia and terminal velocity, making the droplet-turbulence interaction nonlocal and multiscale in nature. Therefore, interactions between cloud dynamics and cloud microphysics in a turbulent cloud represent complex multiscale and multiphase problems (**Figure 1**).

This complex physics inspired Shaw (2003) to write a review paper on the very subject for the fluid mechanics community, in which many open issues were discussed along with results from preliminary studies before 2003. Over the past 10 years, there has been a surge of research publications in this area thanks to better computational research tools and better instrumentation for observations. Although there are still many open issues, the progress in the past 10 years has led to a better quantitative understanding of the effects of turbulence, which we summarize

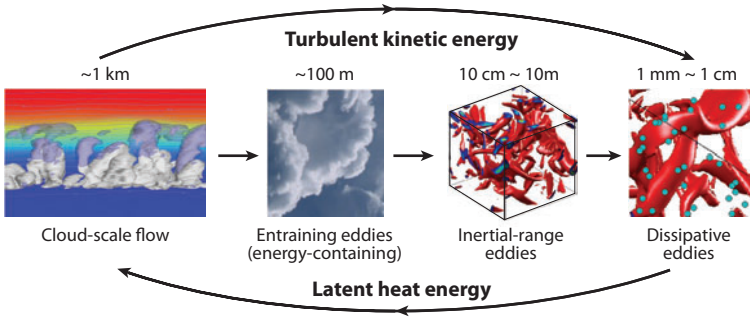

Figure 1

Multiscale interactions in atmospheric clouds. The turbulent kinetic energy flows from cloud-scale motion to dissipative eddies. Latent heat energy flows from individual droplets to cloud-scale motion.

in this review. In the same time frame, there has been closer collaboration between the fluid mechanics community and the atmospheric sciences community, with several workshops in the United States and Europe (e.g., 2008 Physics of Climate Change workshop, Kavli Institute for Theoretical Physics, University of California, Santa Barbara; 2008 Dynamics of Inertial Particles: From Ocean and Atmosphere to Planets workshop, Max Planck Institute, Dresden; 2009 Clouds and Turbulence workshop, Imperial College London; and 2010 International School on Fluctuations and Turbulence in the Microphysics and Dynamics of Clouds, France). The 2009 Imperial College London workshop led to a recent thorough review of work over the past two decades (Devenish et al. 2012). Our review differs from Devenish et al. (2012) in that we provide a more succinct physical description of the cloud physics problem for the engineering fluid mechanics community and also more detailed interpretations of some of the quantitative differences in recent published studies to better illustrate open research issues. Other relevant reviews, focusing on various aspects of cloud physics and the effects of cloud turbulence, are those by Beard & Ochs (1993), Jonas (1996), Vaillancourt & Yau (2000), and Khain et al. (2007).

2. CHARACTERISTICS OF TURBULENCE AND DROPLETS IN WARM CLOUDS

2.1. Air Turbulence and Droplet Characteristics

A warm cloud consists of moist air, aerosol particles, and liquid droplets. The size of background aerosol particles is typically much less than 1 μm, with mass concentration in the range 10–100 μg m^{-3}, and their direct effect on the fluid dynamics of clouds is negligible. The number concentration of aerosol particles serving as CCN affects the concentration of liquid droplets. The radius of cloud droplets is typically in the range 1–20 μm, with volume and mass fractions of $\sim 10^{-6}$ and $\sim 10^{-3}$, respectively. Therefore, the presence of cloud droplets has a negligible effect on the air turbulence. However, when water vapor condenses or evaporates from cloud droplets, the mass and energy transfers between the moist air and the dispersed phase are crucial for the dynamics of clouds through the buoyancy effect.

Air turbulence in clouds is characterized by large flow Reynolds numbers, small energy dissipation rates (relative to many engineering flows), moderate velocity fluctuations, and a wide inertial subrange (Shaw 2003). The dissipation rate ε is a key parameter and depends on the cloud type and age, with values around 10^{-3} m^2 s^{-3} in stratocumuli, 10^{-2} m^2 s^{-3} in cumuli, and 10^{-1} m^2 s^{-3}

or higher in cumulonimbus clouds (e.g., Jonas 1996, Pruppacher & Klett 1997). The root-mean-square velocity u' is typically $\sim$1 m s^{-1} and appears to increase with ε (MacPherson & Isaac 1977, table 1). Let us take a typical value of $u' = 1$ m s^{-1} and $\varepsilon = 0.01$ m^2 s^{-3}, the Taylor microscale Reynolds number $R_\lambda \sim u'^2\sqrt{15/\nu\varepsilon} \sim 10^4$; the integral length scale $l \sim u'^3/\varepsilon \sim 100$ m (the scale of entraining eddies); and integral timescale $T_e \sim l/u' \sim 100$ s. In contrast, the Kolmogorov length η is equal to $(\nu^3/\varepsilon)^{0.25} \sim 0.8$ mm, time $\tau_k = (\nu/\varepsilon)^{0.5} \sim 0.04$ s, and velocity $v_k = (\nu\varepsilon)^{0.25} \sim 2$ cm s^{-1}. Therefore, typical scale separations are $l/\eta \sim 10^5$, $T_e/\tau_k \sim 2{,}500$, and $u'/v_k \sim 50$. We note that the smallest scales governing the temperature and water-vapor fluctuations (i.e., Batchelor scales) are similar to η as the thermal diffusivity κ of air and the diffusivity D_w of water vapor are similar in magnitude to the kinematic viscosity ν of air, with $\nu/\kappa \approx 0.71$ and $\nu/D_w \approx 0.60$ under atmospheric conditions (Montgomery 1947). This highlights the multiscale interactions mostly in terms of length scales and timescales (**Figure 1**).

Cumulus clouds: the most common type of warm cloud with clearly defined edges, having a puffy or cotton-like appearance

FSSP: Forward Scattering Spectrometer Probe

Although cloud droplets are small ($r < \eta$), their motion is tightly coupled with the air turbulence. This can be seen by comparing the droplet Stokes inertial response time $\tau_p = 2\rho_p r^2/(9\mu)$ and still-fluid terminal velocity $v_p = \tau_p g$ to the Kolmogorov scales, where r is the droplet radius, μ is the air viscosity, ρ_p is the water density, and g is the gravitational acceleration. For droplets with radii 10 μm $< a <$ 60 μm, the Stokes number varies from 0.01 to 2, and the nondimensional settling parameter v_p/v_k varies from 1 to 40 (Ayala et al. 2008b, figure 1). Hence the gravitational settling is almost always important, whereas the inertial effect is weak for small ε and significant for large ε. Both parameters increase rapidly with droplet size, which demonstrates the strong nonlinear nature of droplet-turbulence interactions.

One needs also to keep in mind that cloud turbulence most likely exhibits strong large-scale inhomogeneity and nonstationarity. For instance, interfacial instabilities responsible for the cauliflower-like appearance of cumulus clouds provide a strong and intermittent source of turbulent kinetic energy (see Grabowski & Clark 1993). Moreover, there might also be subtle differences between the characteristics of dry and cloudy-air turbulence, as suggested by numerical experiments (e.g., Spyksma & Bartello 2008).

2.2. Cloud Observations Relevant to Turbulence Effects

Observing the wide range of scales relevant to cloud dynamics from an aircraft is challenging because of the aircraft speed ($\sim$100 m s^{-1}). This requires instruments with extremely fast response times. Even if appropriately fast instruments are available, they need to be located close to each other to provide useful information about small-scale cloud structures. Moreover, the presence of cloud droplets makes it difficult to accurately measure such fundamental cloud properties as temperature or water vapor because of instrument wetting. The same issue applies to measurements of turbulence characteristics using hot-wire anemometers (e.g., Siebert et al. 2007).

The spatial distribution of cloud droplets (e.g., due to inertial small-scale clustering, the preferential concentration) continues to be a topic of considerable interest. Studies have applied cloud data collected by the Fast Forward Scattering Spectrometer Probe [(Fast FSSP) Brenguier 1993]. Chaumat & Brenguier (2001) argued that small-scale concentration inhomogeneities in close-to-adiabatic (i.e., weakly affected by entrainment and mixing) cloud volumes were small compared to purely random (i.e., Poisson) statistics. A similar conclusion was reached by Kostinski & Shaw (2001, figure 3), who argued that the weak effect they observed resulted from the small dissipation rate within the cloudy segment analyzed (around 10^{-4} m^2 s^{-3}; such a value is small but not atypical for close-to-adiabatic regions of a small convective cloud). In contrast, Pinsky & Khain (2003) observed significantly larger effects (i.e., centimeter-scale concentration fluctuations in the range 5–30%). Their analysis, however, did not focus on close-to-adiabatic parts of cloud traverses but

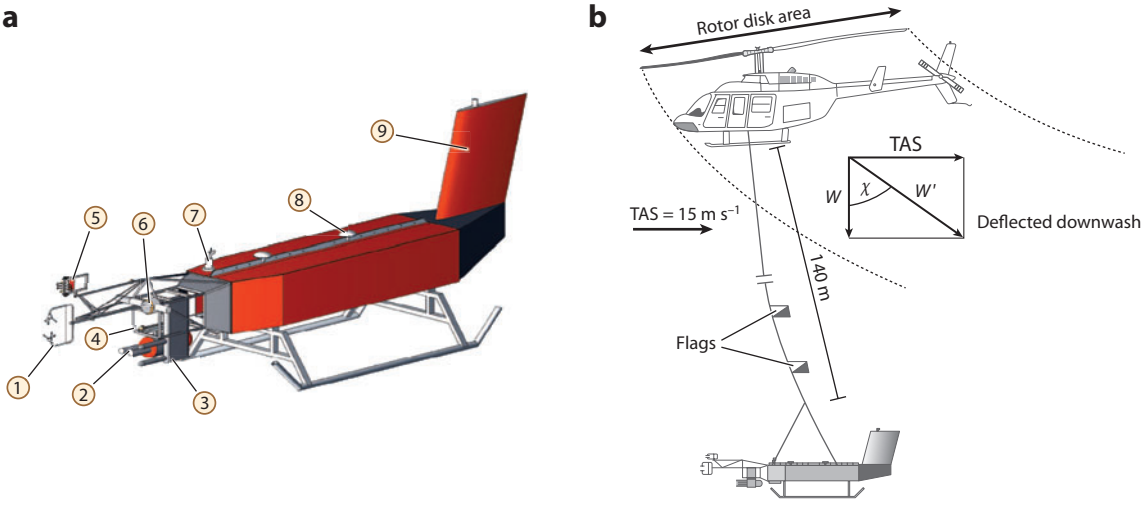

Figure 2

(*a*) Sketch of the Airborne Cloud Turbulence Observation System (ACTOS): (*1*) sonic anemometer; (*2*) M-Fast Forward Scattering Spectrometer Probe (FSSP); (*3*) phase-Doppler interferometer; (*4*) impactor inlets; (*5*) Ultra-Fast Thermometer (UFT); (*6*) Particle Volume Monitor (PVM-100A); (*7*) Nevzorov probe; (*8*) the main body consisting of five covered 19-inch racks including electronics, data acquisition, power supply, and dGPS antenna; and (*9*) the tail unit. (*b*) ACTOS suspended from a Bell Long Ranger helicopter when taking measurements. Abbreviation: TAS, true air speed. Figure reproduced with permission from Siebert et al. (2006b).

included cloud volumes significantly affected by entrainment. In nonadiabatic cloudy volumes, concentration heterogeneities can originate from the turbulent stirring of initially coarsely mixed cloudy and clear-air volumes.

The Ultra-Fast Thermometer (UFT) developed at the University of Warsaw (Haman et al. 1997, 2001; Rosa et al. 2005) provides temperature measurements at scales down to a few centimeters when mounted on a research aircraft. The Particle Volume Monitor (PVM-100A) is a cloud probe that samples liquid water content (LWC) in a volume of approximately 1 cm^3 with frequencies of up to 5 kHz (i.e., every 2 cm at an aircraft speed of 100 m s^{-1}) (Gerber et al. 1994). The combined use of the UFT, Fast FSSP, and PVM-100A makes it possible to probe small scales of the temperature and LWC within clouds. However, these probes are often located several meters apart (e.g., Haman et al. 2007), which severely limits investigations of small-scale cloud structures, as explained above.

Significant progress in observing small-scale cloud structures, including characteristics of the velocity field, has come from the development of the Airborne Cloud Turbulence Observation System (ACTOS) (Siebert et al. 2006b; see **Figure 2**). ACTOS includes a suite of cloud probes, including Fast FSSP, UFT, and PVM, as well as an ultrasonic anemometer, among other instruments. The instruments are positioned within close proximity to each other. ACTOS was initially flown using a tethered balloon (Siebert et al. 2006a) and more recently using a helicopter (Siebert et al. 2006b). The clear advantage of a helicopter-borne measurement system is the significantly lower horizontal speed that only needs to be sufficiently large to avoid the downwash reaching the instrument platform. However, there is a limited flight ceiling, and typically helicopters are not allowed to fly through clouds. Because of the latter, helicopter applications of the ACTOS platform are limited to cloud-top regions.

ACTOS provided the first reliable small-scale turbulence measurements in clouds as well as corresponding cloud microphysics measurements (e.g., Siebert et al. 2006a, 2010; Lehmann et al.

UFT: Ultra-Fast Thermometer

PVM: Particle Volume Monitor

LWC: liquid water content

ACTOS: Airborne Cloud Turbulence Observation System

2009). These measurements documented that the structure of the velocity field inside studied clouds (shallow cumulus in Siebert et al. 2006a and stratocumulus in Siebert et al. 2010; mean dissipation rates of 10^{-3} and 10^{-4} m^2 s^{-3}, respectively) was close to the homogeneous isotropic high–Reynolds number turbulence down to the smallest scales resolved (~10 cm). Arguably, one might expect some departures from isotropy, which have been demonstrated to occur at centimeter scales (Malinowski et al. 2008). Another relevant aspect is that measured turbulence dissipation rates (estimated by analyzing flight segments approximately 10 m long) were shown to locally follow a log-normal distribution (Siebert et al. 2006a), although in general the form of the probability density function (PDF) of the local dissipation rate could deviate from log normal (Meneveau & Sreenivasan 1991).

PDF: probability density function

Adiabatic parcel: a small volume of air that does not exchange energy (e.g., through radiative processes) or mass (e.g., owing to entrainment) with its environment

3. TURBULENT DIFFUSIONAL GROWTH

3.1. The Adiabatic Parcel Model

The textbook description of the growth of cloud droplets by the diffusion of water vapor involves the concept of an adiabatic cloudy air parcel. The parcel contains cloud droplets that grow or evaporate in response to the vertical motion of the parcel. Elementary considerations allow one to derive the evolution equation for the supersaturation S ($\equiv e_v/e_{vs} - 1$, the relative excess of the water-vapor partial pressure e_v over its saturated value e_{vs}) that describes the balance between the source of S resulting from adiabatic expansion or contraction (due to the parcel's vertical motion in the stratified environment) and the removal of S due to the growth of cloud droplets:

$$\frac{dS}{dt} = a_1 w - \frac{S}{\tau}, \tag{1}$$

where w is the parcel's vertical velocity, a_1 is a coefficient that slowly decreases with the temperature T (from approximately 1.1×10^{-3} m^{-1} for $T = 203$ K to approximately 3.6×10^{-4} m^{-1} for $T = 303$ K) and $\tau = 1/[a_2 N \langle r \rangle]$ is the phase relaxation timescale, with N the droplet concentration, $\langle r \rangle$ the mean droplet radius, and a_2 a coefficient that weakly depends on the air temperature T and pressure P (varying between $\sim 2.7 \times 10^{-4}$ m^2 s^{-1}, for $T = 303$ K and $P = 1{,}000$ hPa, and 3.2×10^{-4} m^2 s^{-1}, for $T = 223$ K and $P = 100$ hPa) (Squires 1952; Politovich & Cooper 1988, equation 1; Shaw 2003, equation 3). The phase relaxation timescale is the characteristic time over which the supersaturation perturbations (i.e., due to changes in the vertical velocity) adjust to the quasi-equilibrium value S_{qe} given by $dS/dt = 0$; that is, $S_{qe} = a_1 w \tau$. Assuming that the velocity w is constant and $S = S_0$ at $t = t_0$, the solution to Equation 1 is

$$S(t) = S_{qe} + (S_0 - S_{qe})\ \mathrm{e}^{-(t-t_0)/\tau}. \tag{2}$$

Table 1 shows approximate values for τ and S_{qe} for representative conditions for small tropical or subtropical cumuli ($T = 283$ K, $P = 800$ hPa, and $w = 1$ m s^{-1}). Both the radii of cloud droplets and their concentrations significantly affect τ and S_{qe}. Typically larger droplet concentrations are associated with smaller droplet sizes; thus the values near the lower-left to upper-right diagonal are most representative for atmospheric clouds. As the table shows, τ is generally in the range 0.1–10 s, with typical values between several tenths of a second and several seconds. The supersaturation adjusts relatively quickly to the quasi-equilibrium values, an aspect of significant consequence, as discussed below in this section. The quasi-equilibrium supersaturations range from 0.01 to 1% for the assumed vertical velocity of 1 m s^{-1} (for different updrafts, the values in the table need to be simply multiplied by w in meters per second). Typical values, again along the diagonal, are between a few hundredths and a few tenths of 1%. Therefore, the adiabatic parcel generally stays close to the water saturation, and such conditions are approached relatively fast, except in

Table 1 Approximate values of the phase relaxation timescale τ (in seconds) and quasi-equilibrium supersaturation S_{qe} (in percentages) for the updraft speed of 1 m s^{-1} and for different combinations of the droplet concentration and droplet mean radius

	Droplet concentration (cm^{-3})			
Droplet radius (μm)	50	100	300	1,000
5	13.3 s	6.7 s	2.2 s	0.67 s
	0.72%	0.36%	0.12%	0.037%
10	6.7 s	3.3 s	1.1 s	0.33 s
	0.36%	0.18%	0.060%	0.018%
15	4.4 s	2.2 s	0.74 s	0.22 s
	0.2%	0.12%	0.040%	0.012%

Coefficients a_1 and a_2 are taken as 5.4×10^{-4} m^{-1} and 3.0×10^{-4} m^2 s^{-1} corresponding to $T = 283$ K and $P = 800$ hPa.

regions where cloud droplets form through the activation of CCN (e.g., Politovich & Cooper 1988). We do not discuss CCN activation in this review, except to note that cloud droplets form through CCN activation at the cloud base as well as above it (the latter because of entrainment or increasing updraft speed) (see Slawinska et al. 2012).

3.2. Supersaturation Fluctuations

The key assumption in the above analysis is that all cloud droplets are exposed to the same supersaturation. This is not necessarily the case if droplets are not homogeneously distributed in space, there is a range of droplet sizes, or there are small-scale vertical velocity fluctuations within the parcel. In those situations, individual droplets are expected to experience different supersaturations. One then may consider the growth of individual droplets within the parcel because only then does the problem become well posed. This was first pointed out by Srivastava (1989), who compared the macroscopic supersaturation (e.g., the parcel mean, as in the discussion above) and the microscopic supersaturation (i.e., felt by an individual droplet).

Can one study the growth of individual droplets in a numerical simulation that follows a large number of droplets? Cloud droplets grow or evaporate because of the presence of moisture and temperature gradients in their immediate vicinity, and these gradients are responsible for the molecular transport of moisture and energy between the droplet and its immediate environment. One may argue that these gradients need to be resolved to represent the growth accurately. Elementary considerations demonstrate that the moisture and temperature gradients in the droplet vicinity are established rapidly [i.e., with a characteristic timescale of milliseconds or smaller (e.g., Vaillancourt et al. 2001, and references therein)]; thus the steady-state droplet growth equation is accurate enough.

More importantly, the volume affected by these gradients has a radius of approximately 10 to 20 droplet radii. Because the mean volume occupied by a single droplet for typical droplet concentrations is between 1 and 2 mm^3, the volume affected by the gradients is approximately 0.1% of the mean volume or smaller. One can simply neglect molecular transport processes in the immediate droplet vicinity and simulate droplet growth using the classical approach, that is, by applying the supersaturation predicted by the mean (over the volume occupied by the droplet) temperature and moisture fields. In other words, one can simply let droplets grow or evaporate according to the mean conditions within their vicinity, resolved by a model with a grid length of the order of the mean distance between the droplets (see Vaillancourt et al. 2001, appendix).

The simplified approach is the only one feasible in direct numerical simulation (DNS) studies that investigate the effects of small-scale turbulence on the diffusional growth of cloud droplets. Because the Kolmogorov microscale describing small-scale turbulence in atmospheric clouds is comparable to the mean distance between cloud droplets (both are ∼1 mm), the DNS approach is well suited for such investigations.

DNS: direct numerical simulation

3.3. Diffusional Growth in a Turbulent Environment: Effects of Small-Scale Turbulence

Vaillancourt et al. (2002) reported the first DNS study of homogeneous isotropic turbulence carrying a large number of cloud droplets growing by the diffusion of water vapor (i.e., the first multiphase simulation of the cloud microscale). The study considered a small volume (∼1 liter) from the adiabatic (i.e., undiluted) cloud core rising with the mean vertical velocity. The DNS model resolved small-scale turbulent perturbations of the velocity, temperature, and water-vapor mixing ratio and followed 50,000 droplets within a triply periodic computational domain with 80^3 grid cells. Each cloud droplet grew by the diffusion of water vapor with the supersaturation determined by local values of the temperature and water-vapor mixing ratio. The authors performed three sets of simulations, spanning the range of dissipation rates relevant to cloud conditions, around 2, 14, and 160 $cm^2\ s^{-3}$. In contrast to previous studies of particle-laden turbulent flows (see Eaton & Fessler 1994), Vaillancourt et al. included droplet sedimentation. The typical droplet sedimentation velocity is ∼1 $cm\ s^{-1}$ and is comparable to the Kolmogorov velocity scale for typical turbulent dissipation rates in clouds. Only for significantly larger dissipation rates, typical for laboratory experiments with particle-laden turbulent flows, can the sedimentation be neglected (Grabowski & Vaillancourt 1999). The simulations reported by Vaillancourt et al. (2002, figure 5, in particular) clearly show the effects of droplet clustering. However, the effects of the turbulence on the droplet growth are small, if not insignificant: The standard deviation of the initially monodisperse droplet distribution increases very slowly with time, of the order of 0.01 μm per minute.

The key argument of Vaillancourt et al. (2002) is that the negligible effect of the small-scale turbulence can be understood through the rapid rearrangement of droplet positions. In brief, cloud droplets that grow faster at one instant (because the local concentration is smaller and the supersaturation higher) subsequently move to a region where the local concentration is higher and the supersaturation is lower. Such changes occur rapidly, with the autocorrelation of the supersatutaion perturbation for a single droplet typically less than a few seconds (see Vaillancourt et al. 2002, figure 13); the effects average out over time relevant for the droplet growth in a cloud (several minutes or longer). Increasing the dissipation rate of the turbulent kinetic energy does lead to increased preferential concentration and increased dispersion of the instantaneous spatial distribution of the supersaturation perturbations, but the width of the droplet spectrum decreases. The latter occurs because the supersaturation autocorrelation time decreases with increasing turbulence intensity. The key point is that diffusional growth is reversible, in contrast to irreversible growth by collision-coalescence, as discussed below.

Similar simulations reported by Lanotte et al. (2009) led to broadly similar conclusions. Lanotte et al. (2009) performed simulations with the same dissipation rate as Vaillancourt et al. (around 10 $cm^2\ s^{-3}$, which might be considered small but arguably is not atypical for adiabatic cores of small cumuli) and with an increasing number of grid cells (from 64^3 to 512^3), thus increasing the flow Reynolds number (from 40 to 185) and the number of droplets carried by the flow (from 10^5 to 3.2×10^7). Their results confirm Vaillancourt et al.'s conclusions because the width of the droplet spectrum increased from zero to values below 0.01 μm over one large-scale-eddy turnover

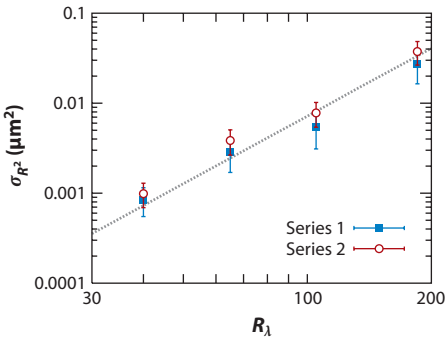

Figure 3

Log-log plot of the standard deviation of the droplet radius squared σ_{R^2} versus the microscale Reynolds number R_λ from DNS simulations. Series 1 and 2 refer to simulations with different liquid water content (1.3 and 0.07 gm^{-3}) and different initial droplet radii (13 and 5 μm). Figure reproduced with permission from Lanotte et al. (2009).

time. However, Lanotte et al. documented a systematic increase of the spectral width with the increasing Reynolds number, that is, with the increase of the computational domain size and thus the range of spatial scales involved (see **Figure 3**). They proposed a simple scaling to extrapolate their results to natural high–Reynolds number turbulent flows, an aspect we return to below in this section.

Celani et al. (2005) performed simulations using a dynamical framework similar to Vaillancourt et al. and Lanotte et al. and reached dramatically different conclusions. In particular, they found a dramatic increase in the width of the droplet spectrum (Celani et al. 2005, figure 3). There are, however, significant differences in their study that make their results uncertain. First, they neglected the latent heating term (i.e., the last term on the right-hand side of Equation 1), which can lead to unrealistically large supersaturation fluctuations, as documented by Vaillancourt et al. (2002), Lanotte et al. (2009), and Sidin et al. (2009). In fact, the probability density function (PDF) of the simulated supersaturation, with values between −4% and 4% (Celani et al. 2005, figure 2), is clearly unrealistic for typical cloud conditions (**Table 1**).

Celani et al. (2007) corrected some deficiencies, but the droplet spectra still showed orders of magnitude larger widths than those of Vaillancourt et al. and Lanotte et al. Celani et al.'s (2005, figure 1; 2007, figure 2) simulations featured extensive cloud-free regions, and as such they do not represent conditions typical in adiabatic cores, in which growing cloud droplets fill the entire volume. Perhaps the main problem is that these simulations, in contrast to those of Vaillancourt et al. (2001, 2002), excluded the mean growth of cloud droplets as the volume under consideration rises inside a cloud. Arguably, Celani et al.'s simulations are more representative of the mixing between cloudy and clear-air volumes (e.g., Andrejczuk et al. 2004, 2006, 2009) than for the adiabatic cloud cores. In summary, careful analysis of these simulations suggests that their relevance to the growth of cloud droplets within adiabatic cloud volumes needs to be treated with much caution.

3.4. Diffusional Growth in a Turbulent Environment: Extension to Large–Reynolds Number Flows

An obvious limitation of DNS studies is the rather limited range of spatial scales involved, often expressed as the relatively small flow Reynolds number. There are two possible implications. First,

the magnitude of the flow Reynolds number affects the magnitude of fluctuations. In particular, infrequent high-amplitude events are key elements of large–Reynolds number turbulence. This was the basis of the argument by Shaw et al. (1998) and Shaw (2000) that long-lasting, strong, small-scale vortices associated with cloud turbulence are regions void of cloud droplets, and thus the supersaturation can build up there and lead to additional activation of CCN or ice initiation. The key aspect, however, is the volume fraction of such structures. If the volume fraction is low, then the effects will be relatively small for the mean cloud properties (see Grabowski & Vaillancourt 1999). Second, one might expect that some flow and/or droplet properties may scale with the Reynolds number as one moves toward larger–Reynolds number turbulence and that such scalings may provide a link between DNS simulations and natural turbulent flows. For instance, Lanotte et al. (2009) suggested a scaling between the width of the droplet spectrum and the Reynolds number deduced from a series of DNS simulations (see **Figure 3**). In principle, such a scaling can be used to extrapolate DNS results to conditions relevant to atmospheric clouds. For instance, if extended to $R_\lambda \sim 10^4$ (a typical value inside natural clouds), the scaling shown in **Figure 3** would imply a standard deviation of the radius squared of $\sim$100 μm^2, more than sufficient to explain spectral broadening observed in clouds.

The scaling shown in **Figure 3**, however, applies only to small eddies and is not valid for eddies significantly larger in size. This is because supersaturation fluctuations, shown to increase with the Reynolds number (see Lanotte et al. 2009, figure 1), approach the quasi-equilibrium value S_{qe}. Because the approach to S_{qe} involves a timescale of the order of 1 s (see **Table 1**), eddies of relatively small spatial scales (compared to the size of a cloud) already have supersaturation values close to S_{qe}. For instance, for a dissipation rate of 10^{-2} m^2 s^{-3} and inertial range scaling, the characteristic velocity u and time t of an eddy of the scale $l = 1$ m are $u = 0.2$ m s^{-1} and $t = l/u = 5$ s. Hence the supersaturations associated with eddies with spatial scales of a few meters or more are close to S_{qe}. In other words, the quasi-equilibrium supersaturation (which only weakly depends on the eddy size as $u \sim l^{1/3}$ for the inertial range scaling) provides a natural break for the supersaturation fluctuations and limits their effect for large eddies. The wide range of eddy sizes raises another aspect that is discussed below in this section.

3.5. Entrainment and Large-Scale Mixing

Because clouds are strongly affected by the entrainment of unsaturated cloud-free air from their immediate environment, especially shallow cumuli (see Warner 1955 and numerous subsequent observational studies; Siebesma et al. 2003), the question is whether entrainment and mixing can significantly affect the droplet spectrum. Entrainment in shallow cumuli has been shown to result in additional activation of entrained CCN (e.g., Brenguier & Grabowski 1993, Slawinska et al. 2012, and references therein), and thus it provides a source of small cloud droplets. Moreover, in addition to the adiabatic effects considered in the DNS studies discussed above, small-scale turbulence and droplet growth can be affected by other processes. Paoli & Shariff (2009) performed DNS simulations similar to those by Vaillancourt et al. (2002) and Lanotte et al. (2009) but added forcing terms at small wave numbers in the temperature and moisture equations, similarly to how the velocity field is forced in DNS studies of homogeneous and isotropic turbulence. Such forcing terms can be argued to result from entrainment and mixing, although entrainment-related processes that lead to temperature and moisture fluctuations at the cloud microscale are significantly more complex [e.g., they involve a gradual filamentation of the coarse cloud and clear-air mixtures (e.g., Andrejczuk et al. 2004, 2006, 2009)]. Nevertheless, the addition of temperature and moisture forcings results in significant fluctuations of the temperature and moisture [with standard deviations around 0.3 K and 1.5×10^{-2} g kg^{-1}, approximately three orders of magnitude

larger than those in the adiabatic case (see Vaillancourt et al. 2002, table 2)] and subsequently fluctuations of the supersaturation field that were two orders of magnitude larger. It is thus not surprising that the mean droplet radius increased from 5 to approximately 5.5 μm, and the standard deviation of the droplet spectrum from zero to approximately 1 μm, within approximately 10 s of the simulation!

Cloud entrainment: process of bringing the unsaturated cloud-free air into the cloud, typically through hydrodynamic instabilities of the interface separating cloudy and cloud-free environmental air

Highly idealized DNS simulations by Paoli & Shariff (2009) illustrate the potential of turbulent entrainment to significantly affect the spectrum of cloud droplets. Cloud entrainment (cumulus entrainment, in particular) is associated with large-scale (i.e., not much smaller than the cloud itself) engulfments that bring subsaturated cloud-free environmental air into the cloud (see, e.g., Grabowski & Clark 1993), in analogy to the entrainment problem in many other natural fluid flows. This process can directly lead to the activation of new droplets on CCN entrained into a cumulus cloud (e.g., Brenguier & Grabowski 1993). It also involves a wide range of scales characterizing the turbulent transport of cloudy air upward within a cumulus cloud. As a result, droplets in the vicinity of a single point follow different trajectories through a turbulent cloud. The key point is that both large and small eddies are needed. Large eddies, with the supersaturation field close to the quasi-adiabatic value S_{qe}, affect the growth of cloud droplets differently in different conditions (i.e., droplet concentration and size, vertical velocity). Small-scale eddies, incapable of affecting the droplet spectrum as described above, are needed to allow droplets to move from one large eddy to another. We refer to this process as large-eddy hopping, in analogy to island hopping (i.e., spending some time on one island and quickly moving to another). Large-eddy hopping results in different growth histories of droplets arriving at a given point in a cloud and affects the observed spectrum.

The concept of large-eddy hopping is not new in cloud physics. Its basic premise was behind the mechanism proposed by Cooper (1989) to explain the disparity between observed droplet spectra and spectra produced in an idealized parcel rising from the cloud base. Cooper developed a simple model describing the effects of various droplet histories and argued that realistic droplet spectra can be obtained by the plausible choice (based on cloud observations) of model parameters. The practical application of the large-eddy-hopping concept to a small cumulus simulation was subsequently developed by Lasher-Trapp et al. (2005) using a two-step procedure (**Figure 4**). First, they simulated a small cumulus cloud by applying a relatively standard cloud model with a simple representation of cloud microphysics. Second, they generated a large ensemble of backward trajectories arriving at a selected point within a cloud (based on model-resolved flow and plausible assumptions concerning parameterized unresolved subgrid-scale motions), and they ran a sophisticated microphysical Lagrangian model along each trajectory. The droplet spectrum at the selected point (the end point of all trajectories) was assumed to come from averaging of final droplet spectra from all trajectories. Lasher-Trapp et al.'s (2005) results document many realistic features of the simulated droplet spectra, such as their large width, the presence of small cloud droplets, and often a bimodal shape. More recent results, including a discussion of beneficial impacts on coalescence initiation, have been presented by Cooper et al. (2011).

Sidin et al. (2009) presented an idealized model encapsulating the idea of large-eddy hopping. The authors followed the growth of cloud droplets through a synthetic turbulent flow field comprising 200 random Fourier modes covering a range of scales, from the integral scale (assumed to be ∼100 m) to the Kolmogorov scale (∼1 mm). The methodology was similar to that of Lasher-Trapp et al. (2005) and involved calculating the droplet growth along a large number of droplet trajectories and averaging the spectra over a sampling area containing end points of the trajectories. Unfortunately, it is difficult to apply the results to realistic cloud conditions owing to some of the model assumptions (e.g., neglecting the latent heating term in the simplified condensation model that leads to unrealistic supersaturation perturbations, as discussed above) and the selection

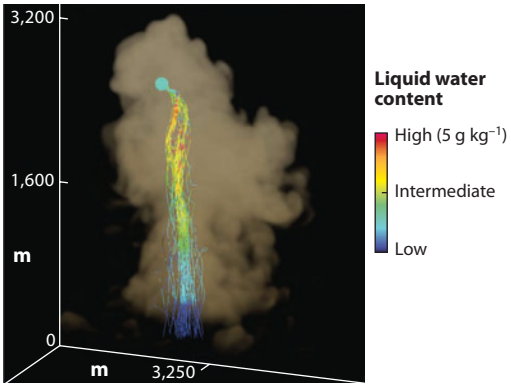

Figure 4

Simulation of a small cumulus, illustrating the idea of cloud-droplet growth through large-eddy hopping. The figure shows the cloud water field and a small subset of droplet trajectories arriving at a single point at the upper part of a cloud. The cloud is evolving, and the cloud shape corresponds to the time at which the trajectories meet at the final location. The trajectories are colored according to the liquid water content encountered. The variability of the vertical velocity across the cloud base already results in some differences in the concentration of activated cloud droplets at the starting point of the trajectories. Some of the trajectories show loops associated with large eddies. There are also relatively small-scale changes in color along the trajectories, highlighting variable environments in which the droplets grow. Figure courtesy of S. Lasher-Trapp.

of parameters for specific simulations (e.g., unrealistic droplet concentration of 8 cm^{-3} in their figure 11).

Sidin et al.'s (2009) results did show some relevant trends that have important implications for future studies. First, results from the appropriate (two-way coupled) simulation showed that spectral broadening significantly depended on the assumed droplet concentration (Sidin et al. 2009, figure 13). This can be understood as the impact of the concentration on the quasi-equilibrium supersaturation S_{qe} within large eddies. Low/high droplet concentration leads to a higher/lower S_{qe}, which affects the spread among various trajectories. One should also anticipate small-scale fluctuations of the droplet concentration owing to droplet inertia (as highlighted in the DNS studies discussed above, but also present in synthetic turbulent flows, as discussed in Pinsky et al. 1999a). Such effects, excluded by Sidin et al., should lead to an additional broadening of the droplet spectrum because of the impact of the droplet concentration on the supersaturation field (see Equation 1). Second, the averaged spectrum was found to be sensitive to the size of the sampling area (Sidin et al. 2009, figure 14). This aspect has obvious implications for the interpretation of aircraft cloud observations that typically involve significant spatial averaging.

In summary, small-scale turbulence alone cannot lead to a significant broadening of the cloud-droplet spectrum. This is because the rearrangement of droplet positions is fast (~1 s), and the effects of enhanced and suppressed growth at small scales average out for times typical for a rise of a cloudy parcel through a cloud (~1,000 s). The small-scale turbulence is the key to large-eddy hopping because it allows individual droplets to move from one large eddy to another. Different activations and growth histories lead to a significant spectral broadening.

4. TURBULENT COLLISION-COALESCENCE

Arenberg (1939) was the first to recognize qualitatively that air turbulence can increase the relative motion and collision rate of cloud droplets, followed by semianalytical studies of Gabilly (1949)

Collision kernel: the collision rate normalized by the relevant pair concentration; also called the collection kernel

and East & Marshall (1954). Saffman & Turner (1956) developed a theoretical formulation for the enhanced relative motion by turbulence on collision rates, applicable to weak-inertia droplets. Reuter et al. (1988) introduced a stochastic model and showed that turbulent fluctuations could enhance the geometric collision kernel. Another aspect studied in the context of cloud droplets concerns the effect of turbulent motion on the collision efficiency of cloud droplets (de Almeida 1976, 1979; Grover & Pruppacher 1985; Koziol & Leighton 1996). These earlier studies are limited in terms of their quantitative capabilities either because of the assumptions made to simplify the equation of motion of droplets or because of the inaccurate methods employed to describe the turbulent fluctuations (see Wang et al. 2005). Over the past 15 years, an increasing number of studies have been reported in both the engineering and atmospheric literature concerning the collision rate of inertial particles in a turbulent flow. Here we survey recent studies addressing the conditions directly relevant to cloud droplets.

4.1. Gravitational Collision-Coalescence

We start with the textbook description of gravitational collision-coalescence, which is still used in most weather and climate models. Because of the relatively low volume fraction of cloud droplets, collision-coalescence is primarily a binary local interaction of droplets. Each coalescence reduces the number of droplets by one count but conserves the total liquid mass. Let us consider the collision-coalescence rate between two given sizes, e.g., of radii r_1 and r_2. The dynamic collision kernel is a rate coefficient defined as $K_{12}^D = \langle \dot{\mathcal{N}}_{12} \rangle / [\langle n_1 \rangle \langle n_2 \rangle]$, where $\langle \dot{\mathcal{N}}_{12} \rangle$ is the average number of collisions observed per unit time per unit volume, and $\langle n_1 \rangle$ and $\langle n_2 \rangle$ are the average number densities. Detecting the dynamic collision kernel directly has only been shown feasible in DNS.

For droplets sedimenting in quiescent background air, larger drops grow in size by colliding with smaller drops. The collision kernel can be expressed kinematically as

$$K_{12}^g = \pi R^2 |W_1 - W_2| \Gamma_{12}^g E_{12}^g, \tag{3}$$

where $R = r_1 + r_2$ is the geometric collision radius, W_1 and W_2 are the terminal velocities of droplets, $\Gamma_{12}^g = \pi R_2 |W_1 - W_2|$ is the gravitational geometric collision kernel, and E_{12}^g is the gravitational collision efficiency (Pruppacher & Klett 1997). The accuracy of the kernel rests on the specification of the terminal velocity as a function of droplet size and the collision efficiency as a function of r_1 and r_2. Typically, the comprehensive model of Beard (1976) is used for W, which considers the Cunningham correction for small droplets and empirical correlations for the effects of nonlinear drag and drop deformation for large drops. The collision efficiency is given either by empirical fitting (Long 1974) or by interpolation from tabulated data (Hall 1980). The Hall collision-efficiency data are believed to be more accurate than Long's empirical formulation. The gravitational kernel is by itself a complex nonlinear kernel whose magnitude can vary by five to six orders of magnitude in the droplet-size range of 10 μm to 1 mm (Xue et al. 2008).

4.2. The Kinematic Formulation of Turbulent Collisions

The quantitative understanding of the turbulent collision of cloud droplets in recent years has been derived primarily from DNS (recently reviewed in Wang et al. 2009). The unique advantage of DNS is that the dynamic collision kernel and the kinematic pair statistics relevant to the collision rate can be simultaneously obtained; such a capability has not been realized in physical experiments. A major result from DNS is the generalized kinematic formulation of the turbulent

geometric collision kernel

$$\Gamma_{12}^{t} = 2\pi R^2 \langle |w_r(r = R)| \rangle g_{12}(r = R), \tag{4}$$

where w_r is the radial relative velocity (RRV) at contact, which combines the differential sedimentation and turbulent transport, and g_{12} is the radial distribution function (RDF) or pair-distribution function that quantifies the effect of local droplet clustering on the average pair density (Sundaram & Collins 1997; Wang et al. 1998, 2000). The RDF is a concept from statistical mechanics and was first introduced by Sundaram & Collins (1997) to quantify the collision rate of inertial particles. This formulation extends the classical spherical formulation of Saffman & Turner (1956) and is valid for all collision mechanisms (Wang et al. 1998). This kinematic formulation has been validated against the DNS dynamic collision kernel, for the geometric collision of nonsedimenting inertial particles (Zhou et al. 2001), and for sedimenting cloud droplets (Ayala et al. 2008b). It forms the basis of the theoretical parameterization of the collision kernel. We emphasize that the relative pair statistics of cloud droplets, governed mostly by small-scale turbulence, are of concern here. Single-particle statistics are often governed by large-scale turbulent motion and may not be directly relevant. We now discuss four documented effects of air turbulence according to the kinematic formulation (Equation 4).

RRV: radial relative velocity

RDF: radial distribution function

4.3. The Effect of Turbulence on the Radial Relative Velocity

The turbulent transport effect concerns the effect of the local shear and air acceleration on the relative fluctuating motion of droplets. Considering only the Stokes drag, inertia, and gravity, and assuming $|\mathbf{r}| \ll \eta$, one finds that the relative velocity between a particle pair at separation $\mathbf{r}$ is governed by

$$\begin{aligned} w_r \equiv \left[\mathbf{V}^{(1)}(t) - \mathbf{V}^{(2)}(t)\right] \cdot \frac{\mathbf{r}}{r} &= \left[\tau_p^{(1)} - \tau_p^{(2)}\right] g \cos\alpha + \frac{r_i r_j}{r} s_{ij} \\ &- \frac{r_j}{r}\left[\tau_p^{(1)} \frac{dV_j^{(1)}(t)}{dt} - \tau_p^{(2)} \frac{dV_j^{(2)}(t)}{dt}\right], \end{aligned} \tag{5}$$

where $\mathbf{V}(t)$ and $\mathbf{Y}(t)$ are the particle velocity and position, respectively; the superscript denotes the specific particle in the pair; and α is the angle between the separation vector $\mathbf{r} = \mathbf{Y}^{(1)}(t) - \mathbf{Y}^{(2)}(t)$ and the gravity direction. The first term on the right-hand side denotes differential sedimentation. The second term is the local fluid shear effect, which depends only on the local flow strain rate s_{ij}. The third term represents the contribution from the particle differential acceleration and is a source of major analytical difficulty.

The key question concerns the magnitudes of the second and third terms relative to the first term. The ratio of the second term to the first term scales as

$$\frac{R}{\eta} \frac{v_k}{\tau_k g} \frac{1}{\cos\alpha \left[St^{(1)} - St^{(2)}\right]} \approx \frac{\sqrt{\nu\varepsilon}}{222.2g\,[r_1 - r_2]} \frac{1}{\cos\alpha}, \tag{6}$$

where the water-to-air density ratio is assumed to be 1,000, and ν is the air kinematic viscosity (Wang & Grabowski 2009). When $r_1 - r_2 = 10$ μm, the ratio is 1.9%, 3.8%, and 6.0% for $\varepsilon = 100$, 400, and 1,000 cm^2 s^{-3}, respectively. An important aspect is that, unlike gravity, the turbulent shear effect makes a finite contribution to the relative motion, even for a pair with identical size.

Assuming the droplet Stokes number $St^{(i)} = 222.2(r_i/\eta)^2 \ll 1$, one may approximate the droplet acceleration by the local fluid acceleration. Then the ratio of the third term to the first

term is roughly

$$\frac{|D\mathbf{U}/Dt|}{g\cos\alpha} \sim \sqrt{\frac{11+7R_\lambda}{205+R_\lambda}}\frac{\varepsilon^{0.75}}{g\nu^{0.25}\cos\alpha}, \tag{7}$$

Flow intermittency: deviation from the Gaussian distribution of velocity gradients, causing the occurrence of very large magnitudes in isolated regions and increasing high-order moments

where the fluid acceleration scaling is taken from Zaichik et al. (2003), which incorporates flow intermittency (see also Ayala et al. 2008a, section 2.1). For $\varepsilon = 100$ cm^2 s^{-3}, the ratio is estimated to be 7.5%, 12%, and 13% at $R_\lambda = 100$, 1,000, and 10,000, respectively. When ε is increased to 1,000 cm^2 s^{-3}, the ratio would be 43%, 68%, and 74% at $R_\lambda = 100$, 1,000, and 10,000, respectively.

The above estimates show that the net effect of turbulence on the RRV mostly results from the local acceleration effect. It is likely moderate for a typical cloud dissipation rate but increases with the flow dissipation rate. The above estimated levels of enhancement appear to be consistent with DNS results (Franklin et al. 2005, 2007; Wang et al. 2005; Ayala et al. 2008b). In their DNS for 10–20-μm pairs, Franklin et al. (2005) found that the RRV increased by 0.8%, 7.3%, 15%, and 49% for $\varepsilon = 95$, 280, 656, and 1,535 cm^2 s^{-3}, respectively. They also demonstrated that the RRV increases with both R_λ and ε.

It is important to note that the differential acceleration term contains both contributions from local fluid acceleration and the memory effect due to finite droplet inertia. The latter has been termed the sling effect (Falkovich et al. 2002, Falkovich & Pumir 2007) or random uncorrelated motion (for a detailed discussion, see Devenish et al. 2012, section 4.2.5). This effect could lead to the formation of strong local singularities in which droplets draw energy from different regions of the flow and collide with very different velocities (e.g., Wilkinson et al. 2006, Bec et al. 2010). However, this scenario is unlikely during rain initiation as the Stokes numbers for cloud droplets are relatively small or gravity dominates the relative motion if the Stokes number is not small. Further work is needed in this direction using particle parameters matching those of cloud droplets.

There are some discrepancies in the magnitude of the RRV. Using a statistical flow description, Khain & Pinsky (1997) found that, for droplets with radii less than 30 μm, the turbulence-induced relative velocity was nearly twice the differential terminal velocity. This overestimation might result from the large number of simplifications they applied to the droplet equation of motion, the inaccuracy of the turbulence model, and the related lack of small-scale dynamics. Using a different PDF model (introduced in Pinsky et al. 2004), Pinsky et al. (2006) later concluded that the relative velocity (or, equivalently, the swept volume) for a droplet pair of 10–15-μm radii only increases by less than 4% and 60% for $\varepsilon = 100$ cm^2 s^{-3} and 1,000 cm^2 s^{-3}, respectively, even at $R_\lambda = 2 \times 10^4$. These results contrast sharply with those of Khain & Pinsky (1997) but are consistent with the above estimates and DNS results. Compared to DNS, one advantage of the statistical approach is that it provides a method to address high–Reynolds number effects such as small-scale intermittency, a point we return to in Section 5.

We stress that DNS results, although at low flow Reynolds numbers and with a limited range of scales, do provide the most reliable quantitative data of pair statistics in a turbulent flow to guide the development of theoretical parameterizations (e.g., Zaichik & Alipchenkov 2003; Zaichik et al. 2003, 2006; Ayala et al. 2008a), as the dynamics of both small-scale turbulence and inertial particles is accurately considered. Statistical models, after being properly validated, can be used to extend the parameter space of DNS. Direct experimental measurements of droplet pair statistics at r close to R are still rare but are becoming feasible at r comparable to η (e.g., Salazar et al. 2008).

4.4. The Effect of Turbulence on the Radial Distribution Function

Maxey (1987) showed theoretically that inertial particles tend to accumulate in local regions of low vorticity and high strain rate owing to an inertial bias or the centrifugal effect, which was confirmed

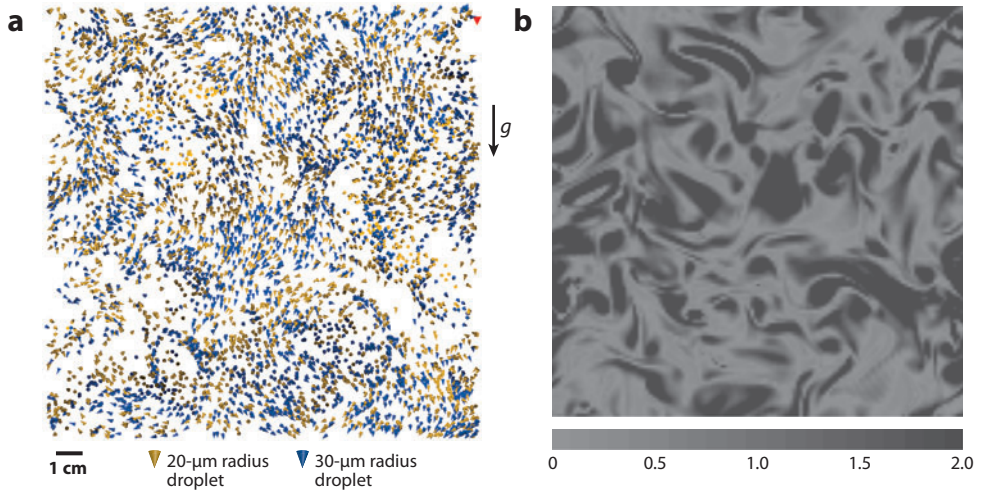

Figure 5

(*a*) A snapshot from DNS of droplet position and (*b*) normalized flow enstrophy on the same planar slice. In panel *a*, the locations of droplets of 20-μm radius are represented by yellow cones and those of 30 μm by blue cones. The flow parameters are $\eta = 0.0592$ cm, $\lambda = 0.991$ cm, $R_\lambda = 72.41$, and $\varepsilon = 400$ cm^2 s^{-3}, and the domain size is 16.8 cm. The 30-μm droplets ($St = 0.570$) show much higher levels of preferential concentration, and 20-μm droplets ($St = 0.253$) display only weak clustering. Figure modified with permission from Ayala et al. (2008b).

in DNS for both nonsedimenting and sedimenting particles (Squires & Eaton 1990, Wang & Maxey 1993). Because local collision rates are proportional to the second moment of local droplet concentrations, the preferential concentration may significantly increase the local pair density as measured by the RDF in Equation 4. However, this connection between droplet clustering and g_{12} is evident only for monodisperse droplets, as in this case $g_{11} \approx \langle n^2 \rangle / (\langle n \rangle)^2$ (Wang et al. 2000). For bidisperse droplets, instead we may write approximately $g_{12} = 1 + \rho_{12}\sqrt{(g_{11} - 1)(g_{22} - 1)}$, where ρ_{12} is the correlation coefficient of the two concentration fluctuations $n_1' \equiv n_1 - \langle n_1 \rangle$ and $n_2' \equiv n_2 - \langle n_2 \rangle$ (Zhou et al. 2001). In the limit of small ρ_{12}, the link between droplet clustering and g_{12} is weak. Indeed, a small difference in droplet radii can result in a rapid decorrelation (Wang et al. 2006a), which is further enhanced by the gravity effect (Woittiez et al. 2009). There have been numerous studies on droplet clustering, especially for monodisperse nonsedimenting particles (reviewed in Khain et al. 2007, Ayala et al. 2008a, Devenish et al. 2012). The discussion below focuses on studies of g_{12} for sedimenting cloud droplets.

Pinsky & Khain (1997) presented the first study of droplet clustering on the collision rate. Using a two-dimensional (2D) kinematic turbulence model, they showed that atmospheric turbulence can produce a significant drop-concentration inhomogeneity of spatial scales of the order of a few centimeters. The first DNS data of g_{12} in the context of cloud droplets were obtained by Wang et al. (2005), Franklin et al. (2005, 2007), and Ayala et al. (2008b). At $\varepsilon = 400$ cm^2 s^{-3} and $R_\lambda = 72.4$, the monodisperse RDF for 30-μm (20-μm) droplets is $g_{11} = 16.8$ ($g_{22} = 5.09$), showing significant droplet clustering for each radius (e.g., **Figure 5*a***). These levels of the monodisperse RDF are comparable with those found by Sundaram & Collins (1997) and Wang et al. (2000) for nonsedimenting inertial particles, implying that gravity has a negligible effect on the monodisperse RDF for these droplet sizes. However, for larger droplets, gravity may even increase the monodisperse RDF (see Woittiez et al. 2009, figure 2c) because the motion of clustered droplets

is more correlated and large energetic eddies begin to contribute to the clustering. The bidisperse RDF, however, is very moderate ($g_{12} = 1.13$) owing to the rapid decorrelation (i.e., $\rho_{12} = 0.016$ in this example) of concentration fluctuations between slightly different droplet sizes. Therefore, strong droplet clustering produces only a moderate effect on the net collision rate, except for the collision rate of nearly equal-size droplets. These DNS results illustrate the complex dependence of the RDF on droplet sizes and the different behaviors of the bidisperse and monodisperse RDFs.

Whereas there have been numerous theoretical studies of inertia-induced particle clustering (e.g., Devenish et al. 2012) building on the pioneering work of Maxey (1987), no rigorous theory exists to predict the RDF for bidisperse finite-size sedimenting droplets. Most theoretical results concern the derivation of the power-law relationship $g_{11}(r) \sim (\eta/r)^{f(St)}$ for monodisperse nonsedimenting particles in the limit of small St and the dependence of the exponent $f(St)$ on St (see Devenish et al. 2012, section 4.2.2.2). Falkovich et al. (2002, equation 3) developed a heuristic formulation for the bidisperse RDF in which the effect of gravity is modeled as clustering saturation at a separation larger than R. However, their formulation did not consider the rapid decorrelation between different drop sizes. A more rigorous theory for g_{12} was provided by Chun et al. (2005) based on a balance equation between inertia-induced drift and turbulence diffusion. Specifically, their theory demonstrated that the bidisperse RDF is much smaller than the monodisperse RDF owing to a turbulent acceleration diffusion effect. Using DNS data, Ayala et al. (2008a) extended the work of Chun et al. (2005) to include empirically the effect of gravity. Lu et al. (2010) further extended this theory to charged sedimenting droplets and compared their prediction with experimental RDF data. Zaichik & Alipchenkov (2003) and Zaichik et al. (2006) have successfully carried out a PDF-based modeling approach to predict g_{12} for nonsedimenting particles. Unfortunately, as they did not include gravity, their theory cannot be applied to cloud droplets.

4.5. The Effect of Turbulence on the Droplet Settling Velocity and Its Relevance to Collisions

Sedimenting particles bias their trajectories toward regions of downward fluid motion around vortices and could settle significantly faster than the terminal velocity because of this preferential sweeping mechanism (Maxey 1987, Wang & Maxey 1993). Davila & Hunt (2001) constructed a theoretical model based on a 2D Rankine vortex to investigate the mean settling velocity of a single inertial particle. Their most significant conclusion is that the maximum increased settling, normalized by the terminal velocity, occurs when the droplet Froude number

$$F_p = \frac{\tau_p W^2}{\Gamma_{\text{vort}}} = \frac{\tau_p^3 g^2}{\nu} = St S_v^2 \tag{8}$$

is of the order of 1. Here F_p represents the ratio of inertia-induced centrifugal force ($m_p W^3/\Gamma_{\text{vort}}$) to the gravity force ($m_p g$), and Γ_{vort} is the vortex circulation. Interestingly, this parameter is independent of the flow dissipation rate and reaches 1 at a droplet radius of 20.8 μm assuming $\nu = 0.17$ cm^2 s^{-1}. This prediction was confirmed by Ayala et al. (2008b), who showed that the maximum relative increase in the settling velocity did occur at $a \approx 20$ μm, and the level of increase grows with flow Reynolds number (~23% at $R_\lambda = 72$). Ayala et al. also showed that this increase in single-droplet settling ceases when $a > 50$ μm. This size-dependent increased settling led Ghosh & Jonas (2001) and Ghosh et al. (2005) to argue that turbulence could significantly alter the collision-coalescence growth through the modified relative mean motion of droplets in clouds.

However, there might not be a direct connection between the average increased settling of a single droplet and the local differential settling of a droplet pair. The increase in the average

settling of a single droplet can be expressed as

$$\left\langle V_3^{(i)} \right\rangle - \tau_p^{(i)} g = \left\langle U_3 \left[Y^{(i)}(t), t \right] \right\rangle, \tag{9}$$

where we assume that the third coordinate direction is vertically downward (i.e., along the gravity direction), and the angle brackets denote the ensemble average over a droplet path (Wang & Maxey 1993). However, as a colliding droplet pair is always nearby, what is truly relevant to the collision rate is the local differential settling, namely, conditioned on a separation distance equal to R ($R < \eta$),

$$\begin{aligned} \left\{ \left[\left\langle V_3^{(1)} \right\rangle - \left\langle V_3^{(2)} \right\rangle \right] - \left[\tau_p^{(1)} - \tau_p^{(2)} \right] g \right\}_{|\mathbf{r}|=R} &= \left\langle U_3 \left[Y^{(2)}(t) + \mathbf{r}, t \right] \right\rangle - \left\langle U_3 \left[Y^{(2)}(t), t \right] \right\rangle \\ &\approx \left\langle r_j \frac{\partial U_3 \left[Y^{(2)}(t), t \right]}{\partial x_j} \right\rangle_{|\mathbf{r}|=R}, \end{aligned} \tag{10}$$

which clearly depends on the collision radius and is fundamentally different from the change in the differential average settling of single droplets, $\langle U_3[Y^{(1)}(t), t] \rangle - \langle U_3[Y^{(2)}(t), t] \rangle$. The latter poses no constraint on the large droplet position $Y^{(1)}(t)$ relative to the position of the smaller droplet $Y^{(2)}(t)$. The conditional statistics shown in Equation 10 have not yet been studied in DNS. A similar issue related to the last term in Equation 5 should also be studied; namely, the contribution of the particle relative acceleration should be conditioned on the collision radius in order to be directly relevant to the collision rate.

Pinsky et al. (2001) considered a different mechanism concerning the change in the droplet terminal velocity. The droplet terminal velocity can increase with height owing to decreasing ambient air density, which could increase the relative motion between a pair of droplets. The authors showed that an increase of 5% to 20% in the relative velocity is possible, which could lead to a significant increase (up to a factor of 2) in the collision efficiency.

There are other mechanisms that could alter the terminal velocity of inertial particles, such as vortex trapping, the effect of nonlinear drag, and the loitering effect (see Good et al. 2012, section 3.2.2). For cloud droplets, these effects are likely insignificant because of the typical physical conditions in cloud turbulence.

4.6. The Effect of Turbulence on Collision Efficiency

For droplets with radius falling in the size gap, the collision efficiency depends sensitively on the radius and any alteration of the far-field (with separation larger than ~10 radii) and near-field (with separation less than one radius) relative motion (Klett & Davis 1973, Wang et al. 2005). Turbulence alters the distributions of the angle of approach and relative velocity for colliding droplets (Wang et al. 2006b); thus qualitatively we expect turbulence to modify the collision efficiency.

Pinsky et al. (1999b) proposed a mathematical formulation to study the effect of far-field turbulent fluctuations on drop-drop aerodynamic interactions. Working in a frame of reference moving with the local airflow, they added a far-field, inertia-induced turbulence contribution $\tau_p d\mathbf{U}/dt$ to the drop-air relative motion, where $\mathbf{U}$ is the undisturbed local airflow velocity. Their main conclusion is that the collision efficiency in a turbulent flow is a random variable with a mean that is larger than the gravitational collision efficiency. Their formulation, however, relies on a number of assumptions, including that the droplet Stokes number is small, the inertia-induced relative motion has a timescale greater than that associated with drop-drop aerodynamic interactions, and the two interacting drops remain in the same flow eddy during the entire time interval of aerodynamic

interaction. These assumptions are not always valid for high flow dissipation rates or larger droplet sizes. Furthermore, their turbulent flow was kinematically constructed as 2D, frozen, pseudo-turbulence in terms of random Fourier modes. This flow model does not adequately describe the fine structure of a turbulent flow and leads to overestimation of the magnitudes of Lagrangian accelerations, as noted by Pinsky & Khain (2004). Using the same formulation, Pinsky & Khain (2004) studied the effects of fluid accelerations at high flow Reynolds numbers. They showed that the collision efficiency for collector drops exceeding 10 μm can be increased by 25% to 40% at $\varepsilon = 200$ cm^2 s^{-3}, and 2.5 to 5 times at 1,000 cm^2 s^{-3}.

Pinsky et al. (2007) re-examined the effect of turbulence on drop-drop aerodynamic interactions using a different stochastic model for local turbulent velocity gradients and Lagrangian fluid accelerations (i.e., the PDF model of Pinsky et al. 2004) but under similar physical assumptions concerning the dynamics of droplet motion and hydrodynamic interaction as those of Pinsky et al. (1999b). For droplets less than 20 μm in radius, Pinsky et al. (2007) found that turbulence can increase the collision efficiency by up to a factor of 4 at high flow dissipation rates and cloud turbulence Reynolds numbers, which is much greater than the effect of turbulence on the drop-drop relative velocity (i.e., less than a factor of 1.6) (see Pinsky et al. 2006). Their tabulated results of turbulent collision efficiency are presented in Pinsky et al. (2008).

A significant step toward fully coupling the background air turbulence and local disturbance flows induced by droplets was made by Wang et al. (2005a) and Ayala et al. (2007), who developed a hybrid DNS approach to the problem of turbulent collisions of aerodynamically interacting cloud droplets. Their basic idea was to combine DNS of the background air turbulence with analytical Stokes disturbance flows. The approach takes advantage of the fact that the disturbance flow due to the droplets is localized in space within Kolmogorov eddies. This hybrid approach provides, for the first time, a quantitative tool for studying the combined effects of air turbulence and aerodynamic interactions on the motion and interactions of cloud droplets. The disturbance flow is coupled with the background air turbulence through the approximate implementation of the no-slip boundary conditions on each droplet. Dynamical features on spatial scales ranging from a few tens of centimeters down to 10 μm are captured. Both the near-field and the far-field droplet-droplet aerodynamic interactions could be incorporated (Wang et al. 2007a), with possible systematic improvements of their accuracy (Rosa et al. 2011b).

Wang et al. (2005) demonstrated that the kinematic formulation (Equation 4) is still valid for aerodynamically interacting droplets when correcting for the fact that droplets can no longer overlap in space. They showed that the total enhancement factor η_T of the collision rate is a product of the enhancement of the geometric collision, $\eta_G \equiv \Gamma_{12}^t / \Gamma_{12}^g$, and the enhancement of the collision efficiency, $\eta_E \equiv E_{12}^t / E_{12}^g$, where E_{12}^t is the turbulent collision efficiency. The kinematic collision kernel for aerodynamically interacting droplets is then written as

$$K_{12} = \Gamma_{12}^t E_{12}^t = \left(\Gamma_{12}^g \eta_G\right)\left(E_{12}^g \eta_E\right) = K_{12}^g \eta_T . \tag{11}$$

Using this hybrid DNS, Wang et al. (2008) and Wang & Grabowski (2009) found that turbulence could significantly enhance the collision efficiency. The enhancement depends nonlinearly on the size ratio r_2/r_1 and grows with increasing ε. The net enhancement $\eta_T = \eta_E \eta_G$ typically ranges from 1 to 5. It becomes larger when the droplets are rather different in size ($r_2/r_1 \ll 1$) or are nearly equal in size ($r_2/r_1 \to 1$) (see **Figure 6**). When $r_2/r_1 \to 1$, the gravitational kernel is small owing to small differential sedimentation. When $r_2/r_1 \ll 1$, the gravitational kernel may also be small owing to small collision efficiency. Therefore, air turbulence plays an important role in enhancing the gravitational collision kernel when the collision efficiency is small. The values of η_E and η_G from the hybrid DNS have been tabulated by Ayala et al. (2008b) and Wang et al. (2008).

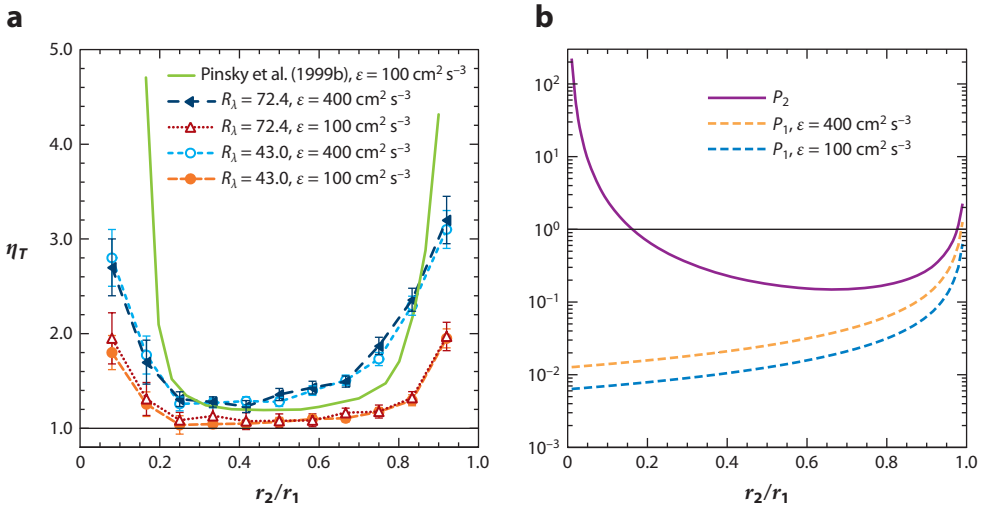

Figure 6

(*a*) The net enhancement factor (the ratio of the turbulent collection kernel and the hydrodynamic-gravitational collection kernel) plotted as a function of the radius ratio r_2/r_1, with the larger droplet 30 μm in radius. ε is the flow viscous dissipation rate, and R_λ is the Taylor microscale Reynolds number of the simulated background turbulent airflow. (*b*) Two scale ratios as a function of r_2/r_1 with $r_1 = 30$ μm, where P_1 is the ratio of the relative velocity due to turbulent shear to the differential terminal velocity, and P_2 indicates the ratio of aerodynamic interaction time to the inertial response time of the smaller droplet. Figure taken with permission from Wang & Grabowski (2009).

4.7. Parameterization of Turbulent Collection Kernel

Before the effects of turbulence can be included in the kinetic collection equation (e.g., Shaw 2003, equation 1) to study droplet growth by collision-coalescence, analytical parameterizations of the turbulent geometric collision kernel and turbulent collision efficiency must be developed. One way to parameterize the turbulence effects is to write $K_{12} = \Gamma^t_{12} E^g_{12} \eta_E$. Ayala et al. (2008a) provided a parameterization for the turbulent geometric collision kernel Γ^t_{12} by combining a theory for $\langle |w_r| \rangle$ and an empirical model for g_{12}. As a first step, the enhancement factor η_E can be interpolated from the tabulated values given by Wang et al. (2008) and Wang & Grabowski (2009). Using this combination, we find that the net enhancement factor η_T reaches a maximum of 2 to 3 at $\varepsilon = 100$ cm^2 s^{-3}, and 4 to 5 at $\varepsilon = 400$ cm^2 s^{-3} (see Grabowski & Wang 2009, figure 2). The relative contributions of various effects of turbulence are noted by Devenish et al. (2012, figure 2), demonstrating that the turbulence effect on the collision efficiency (η_E) is primarily responsible for the enhancement associated with different droplet sizes (i.e., small r_2/r_1), whereas clustering (g_{12}) is mainly responsible for the enhancement for nearly equal sizes ($r_2/r_1 \sim 1$).

Several other parameterizations have been published. Falkovich et al. (2002) developed a semianalytical kernel that includes the effects of droplet clustering and local fluid acceleration due to cloud turbulence. They concluded that turbulence has a significant effect on the geometric collision kernel for droplets with 20- to 60-μm radii. A similar parameterization was presented by Derevyanko et al. (2008), who proposed a model for the enhancement factor due to droplet clustering, applicable to arbitrary droplet Stokes numbers. Franklin (2008) suggested an empirical

parameterization based on the DNS data of Franklin et al. (2007) of the turbulent geometric collision kernel. A limitation of her parameterization is that the flow Reynolds number was assumed to match the conditions in DNS, rather than cloud conditions. Onishi et al. (2009) provided a parameterization of the turbulent geometric collision for monodisperse cloud droplets, focusing on the effect of gravity on the RRV.

Warm rain processes: processes involved in the growth of cloud droplets to produce drizzle and rain, in contrast to precipitation processes associated with the ice phase

DSD: droplet-size distribution

4.8. Impact on Warm Rain Development

The bottom-line question is how the turbulence enhancement affects the time evolution of the droplet-size distribution (DSD) and the rate of conversion of cloud droplets to raindrops. This question has typically been addressed by solving the kinetic collection equation governing the DSD. The droplet size is divided into bins, and the droplet number and mass in each bin are computed in time. The result based on the turbulent collision kernel (K_{12}) is then compared with that based on the gravitational collision kernel (K_{12}^{g}).

Pinsky & Khain (2002) demonstrated that an average turbulence enhancement of 2 to 3 in the collision kernel significantly accelerates the process of rain formation. Falkovich et al. (2002) found that turbulence-induced inertial effects (in particular, droplet clustering) can substantially accelerate droplet growth over the condensation-coalescence size gap. Specifically, they indicated that the number density of newly formed raindrops after 10-min collision interactions was increased from 0.64 cm^{-3} to 1.06 cm^{-3} by turbulence effects, when $\varepsilon = 2{,}880$ cm^2 s^{-3}.

Riemer & Wexler (2005) devised a turbulent geometric collision kernel by simply adding a turbulent kernel for nonsedimenting droplets to the gravitational kernel. This treatment overestimated the turbulent effects, as pointed out by Wang et al. (2006a). As a result, Riemer & Wexler found a significant impact of turbulence even at $\varepsilon = 100$ cm^2 s^{-3}.

Applying an accurate algorithm developed by Wang et al. (2007b), Xue et al. (2008) solved the kinetic collection equation using different collection kernels for an initial distribution with a mean volume radius of 9.3 μm and an LWC of 1 g m^{-3}. They found that, even when η_E is set to 1, the turbulent collision kernel of Ayala et al. (2008a) at $\varepsilon = 300$ cm^2 s^{-3} can shorten the formation time of drizzle drops by approximately 40% relative to the Hall gravitational collection kernel. They devised a methodology to identify the three phases of droplet growth (Berry & Reinhardt 1974): the autoconversion phase, the accretion phase, and the larger hydrometeor self-collection phase. Their key conclusion is that even a moderate enhancement of the collection kernel by turbulence can significantly impact the autoconversion phase of the growth. Hsieh et al. (2009) found that the same turbulent kernel increases the conversion rate of the cloud mass to rain by a factor of 1.82 and 1.24 for two observed cloud DSDs. A similar calculation was performed by Franklin (2008), who found that the amount of mass associated with drop sizes greater than 40 μm in radius after 20 min of growth is 21.4% for the turbulent collision kernel at 100 cm^2 s^{-3}, compared with only 0.9% for the pure gravitational kernel. This demonstrates a substantial acceleration of raindrop formation, and this acceleration increases with the flow dissipation rate.

Wang & Grabowski (2009) repeated the calculations of Xue et al. (2008) but added the effect of turbulence on η_E at $\varepsilon = 400$ cm^2 s^{-3}. They found that the time interval for the autoconversion phase is reduced from approximately 32.5 min (Hall kernel) to only 10.5 min (the turbulent kernel) (see **Figure 7**). If a radar reflectivity factor of 20 dBZ is used as an indicator for drizzle precipitation, the time needed to reach such a reflectivity changes from approximately 2,450 s for the Hall kernel to 1,230 s for the turbulent kernel.

Using a turbulent collection kernel, Pinsky et al. (2008) also integrated the kinetic collection equation. In their calculations, they included the turbulence effects for droplets with $r \leq 21$ μm only because of model limitations. They showed that the turbulent collection kernel leads to the

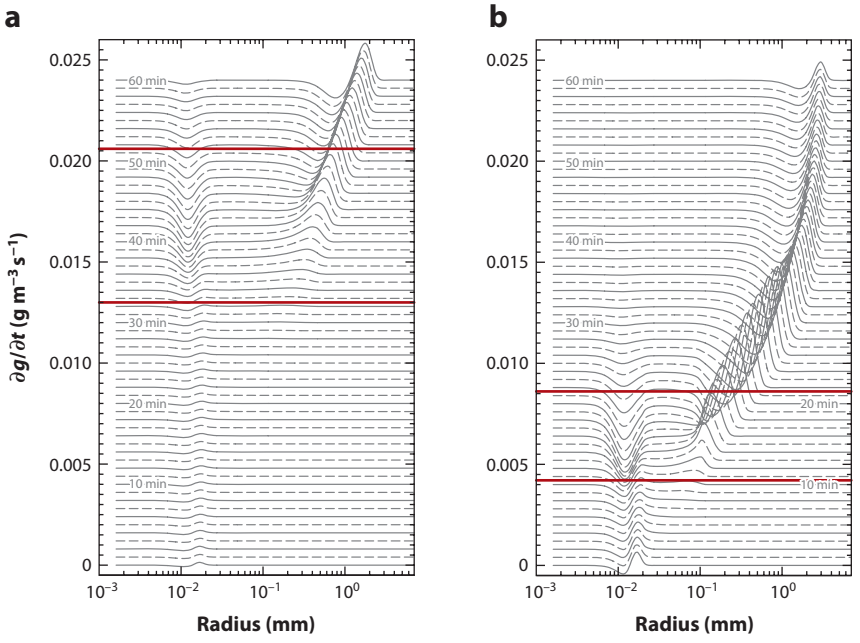

Figure 7

The rate of change ($\partial g/\partial t$, g m^{-3} s^{-1}) of the droplet mass density in each numerical bin as a function of droplet radius: (*a*) solutions using the Hall kernel and (*b*) solutions using a turbulent kernel at a flow dissipation rate of 400 cm^2 s^{-3} and root-mean-square fluctuation velocity of 2.0 m s^{-1}. There are 61 curves (*gray*) in each plot, representing $t = 0$ to 60 min with a time increment of 1 min. Curves alternate between solid and dashed lines to increase the legibility of times, and the curves for $t > 0$ are shifted upward by a constant for clarity. The value of $\partial g/\partial t$ can be either positive or negative, with the total integral over the whole size range equal to zero owing to the mass conservation. At any given time, a positive $\partial g/\partial t$ for a given size bin implies that the mass density for that size bin is increasing. The two red lines mark the beginning and end of the accretion phase. Figure taken with permission from Wang & Grabowski (2009).

production of raindrops after 30 min for almost all cases, except one with a high initial droplet concentration and low flow dissipation, and no raindrops were produced by the gravitational kernel.

Grabowski & Wang (2009) studied the impact of turbulence on rain initiation by applying a rising adiabatic parcel model in which droplet activation, diffusional growth, and turbulent collision-coalescence were considered together. Using the turbulent collection kernel of Wang & Grabowski (2009), they showed that turbulence effects could reduce the rain initiation time by 25% to 40% for typical continental and maritime cloud conditions.

Seifert et al. (2010) conducted large-eddy simulations of small cumulus clouds using the turbulent collision kernel of Ayala et al. (2008a) and found that the turbulent kernel increased rain production. The effect was most pronounced near the cloud top where dissipation rates are higher. They showed that the LWC is correlated with the local dissipation rate.

In summary, recent studies applying DNS and stochastic turbulence models have firmly established that air turbulence can cause a moderate enhancement to the collision kernel (a factor of 2 to 5 for selected droplet sizes and realistic flow dissipation). Interestingly, earlier studies reported both weaker (Saffman & Turner 1956, Koziol & Leighton 1996) and stronger effects (e.g., Tennekes & Woods 1973, de Almeida 1979, Pinsky & Khain 1997), either because of the limited/inappropriate

parameter spaces considered or because of the inconsistent/flawed approaches used. More interesting is the realization that the moderate enhancements associated with clustering, relative motion, and collision efficiency occur when the gravitational collision rate is weak (Falkovich et al. 2002, Wang & Grabowski 2009). For example, clustering and turbulent fluctuation are relatively more effective in causing collision between droplets of similar size when the gravitation kernel is close to zero. The turbulent collision efficiency tends to be significantly higher than the gravitational collision efficiency, especially for droplets of dissimilar size. It is then unsurprising to observe that turbulence effects of moderate magnitudes lead to a significant acceleration of warm rain initiation.

5. OPEN ISSUES AND OUTLOOK

We now summarize key open issues relevant to the impact of turbulence on microphysical processes in warm (i.e., ice-free) clouds. Overall, the problem of droplet growth in turbulent clouds involves multiscale interactions between cloud dynamics and cloud microphysics, and there are specific issues for both diffusional and collisional growth. With regard to the diffusional growth of cloud droplets, two issues require further research. First, large-eddy hopping in turbulent clouds needs to be systematically investigated using high-resolution (i.e., grid length of a few meters) numerical simulations in realistic cloud settings. Simulations discussed by Lasher-Trapp et al. (2005) and Cooper et al. (2011) are cumbersome (owing to the two-step procedure) and merely demonstrate the potential of the Lagrangian trajectory approach. A realistic cloud setup needs to include additional processes, beyond just condensational growth as in Sidin et al. (2009), such as the entrainment and activation of fresh CCN from the cloud environment. When combined with high spatial resolution, the Lagrangian approach to cloud thermodynamics—relatively straightforward for activation and condensation alone (Andrejczuk et al. 2008), but cumbersome when collision-coalescence is included (e.g., Shima et al. 2009, Andrejczuk et al. 2010)—seems to provide an excellent computational method to study the growth of cloud droplets in turbulent clouds.

Second, further studies are needed to quantify the role of entrainment and mixing in the fresh activation of CCN above the cloud base, for instance, in large-scale vortical structures (entraining eddies) (Brenguier & Grabowski 1993). Numerical techniques need to better represent the activation/deactivation of CCN due to entrainment/detrainment or, more generally, the processing of CCN by a cloud. Again, the Lagrangian approach seems to be an attractive alternative to Eulerian techniques traditionally applied in cloud modeling. Moreover, the cloud simulations discussed here typically do not consider the environmental stratification of CCN (concentration, composition, etc.). Such effects can potentially impact droplet spectra in upper parts of a cloud field.

With regard to turbulent collision-coalescence, there are many areas for further research. For example, turbulent collision efficiency makes a dominant contribution to the overall turbulence enhancement for cloud droplets in the size gap. The hybrid simulation approach (Ayala et al. 2007) must be further improved to treat near-field droplet-droplet hydrodynamic interactions (Rosa et al. 2011b). Direct experimental measurements of turbulent collision efficiencies need to be explored. Non-Stokes disturbance flows should be considered for large cloud droplets ($r > 30\,\mu$m). Particle-resolved simulations (e.g., Gao et al. 2012) may offer an alternative if the range of scales can be significantly increased through extreme (e.g., exa, zetta) scale computing. Considering the significant role of droplet clustering, the accurate theoretical parameterization of the RDF for sedimenting droplets at finite Stokes numbers is needed. Particularly relevant is the sensitive dependence of the cross-correlation of concentrations on droplet sizes in a bidisperse system (Section 4.4). Furthermore, the sling or caustics effect on the radial relative velocity in the context of cloud droplets needs to be accurately quantified.

Although experimental measurements of pair statistics such as the RRV and RDF are becoming possible at a separation distance of the order of η (e.g., Warhaft 2009, Lu et al. 2010), innovative measurement techniques should be developed to further reduce the measurable separations down to the scale of the droplet radius. In the meantime, extrapolating experimental data at larger separations to the scale of droplet collision could be aided by numerical simulations. As indicated in Section 4, differential pair statistics cannot be obtained from the difference of single-particle statistics. Specifically, the enhanced settling probably has little effect on the collision rate, unlike what has been speculated (Ghosh & Jonas 2001, Ghosh et al. 2005). Direct computations and comparisons of single-particle and particle-pair statistics are needed to further clarify this important aspect.

Impact studies in more realistic cloud models (i.e., featuring high spatial resolutions, bin microphysics, and CCN activation and deactivation) should be pursued to better understand turbulence effects on the DSD, the conversion rate of cloud droplets to raindrops, warm rain initiation time, and the net precipitation rate. We note that DNS simulations conducted to investigate turbulence effects on droplet collisions typically feature computational domains much smaller than a grid box of a cloud model used to investigate the impact of the turbulent kernel in realistic cloud simulations. This problem should be recognized, and computational methodologies need to be developed to account for this scale separation until the size of the domain in DNS and the grid box in cloud simulations can be matched.

There are general issues common to diffusional and coalescence growth. The first concerns the Reynolds number effect: To what extent do the pair statistics such as the RRV and RDF depend on the flow Reynolds number? Most DNS studies were performed at flow Reynolds numbers much less than those in clouds. There is limited evidence that, for given pair of droplet sizes, only a finite range of turbulence scales can affect the pair statistics (Collins & Keswani 2004, Rosa et al. 2011a). This suggests that the pair statistics saturate with increasing flow Reynolds numbers; additional support comes from similar levels of enhancement obtained recently by Pinsky et al. (2006, 2008) using a stochastic approach applicable to high flow Reynolds numbers.

A controversial issue concerns the effect of flow intermittency (e.g., through the third term in Equation 5) at high flow Reynolds numbers in clouds. Increasingly large local fluid accelerations may occur at higher flow Reynolds numbers. Shaw & Oncley (2001) argued that the local fluid acceleration can be as large as 10 g in cloud turbulence. However, this could be insignificant for the RRV and RDF of cloud droplets for the following reasons: (*a*) Pair statistics are low-order statistics; (*b*) droplet inertia combined with gravity quickly filters out the influence of these short-lived intermittent events; (*c*) the highly intermittent regions occupy an insignificant fraction in space; and (*d*) the contribution to differential pair statistics differs significantly from the difference in single-droplet acceleration statistics. For example, Pinsky & Khain (2004) showed that a more realistic PDF of flow accelerations actually reduced the value of the RRV (by 10–15%) when compared to a Gaussian PDF. Nevertheless, further studies on Reynolds number effects and flow intermittency are needed. Petascale simulations could eventually resolve these issues (Wang et al. 2011).

6. SUMMARY

Throughout this review, we strive to delineate the multiscale nature of cloud microphysical processes and highlight challenges that can be addressed through theoretical analysis, experiments (in situ cloud observations and laboratory studies), and numerical simulation. Clearly, significant progress has been made over the past 10 years. Key results include the following. First, small-scale turbulence alone does not produce a significant broadening of the cloud-droplet spectrum during diffusional growth. The growth by the diffusion of water vapor is reversible, and rapid

small-scale turbulent and gravitational mixing of droplets averages out effects of enhanced and suppressed droplet growth due to small-scale supersaturation fluctuations. Second, small-scale turbulence and larger-scale inertial-range eddies jointly lead to a mechanism referred to as large-eddy hopping, in which individual droplets move from one large eddy to another owing to the action of small-scale turbulence. This coupled small-scale and larger-scale mechanism, combined with larger-scale flow inhomogeneity, entrainment, and fresh activation of CCN above the cloud base, creates different growth histories for droplets arriving at a given point in a cloud. This leads to a significant spectral broadening. Third, the effect of turbulence on the irreversible growth by collision-coalescence has been shown to be significant, with an overall enhancement of a classical (i.e., gravitational) collision kernel that is close to 1 for weak cloud turbulence and as high as 5 in strong turbulence. This moderate level of enhancement is a combined effect of enhanced turbulent collision efficiency, droplet clustering, and modified droplet relative motion. The enhancement is particularly strong for droplets of similar size for which purely gravitational collision-coalescence is ineffective. Finally, preliminary impact studies show that turbulence of moderate magnitudes leads to a significant acceleration of warm rain initiation.

The cloud physics community now accepts the relevance of air turbulence to the diffusional and collisional growth of cloud droplets. Much remains to be done to further our quantitative understanding and to develop accurate parameterizations that can be incorporated into weather and climate models. With upcoming developments in the area of extreme-scale computing (exa, zetta, and beyond) and possibilities to measure processes at the cloud microscale in controlled laboratory settings and field experiments (e.g., the ACTOS platform), we are optimistic that a more complete quantitative understanding will emerge in upcoming years and decades. This is timely considering the increasingly refined simulation of weather and the climate at regional and global scales, which requires improve representations of processes that will never be resolved at their native scale, such as growth of an individual cloud droplet. The multiscale problem of atmospheric moist processes can be an exciting area of research with direct societal benefits. The fluid mechanics community has the potential to significantly contribute to the progress.

DISCLOSURE STATEMENT

The authors are not aware of any biases that might be perceived as affecting the objectivity of this review.

ACKNOWLEDGMENTS

This work was supported by the National Science Foundation (NSF) through grants OCI-0904534, OCI-0904449, and ATM-0730766 and by the National Center for Atmospheric Research (NCAR). NCAR is sponsored by the NSF. B. Rosa provided assistance in generating **Figure 5**, as did Andrzej Wyszogrodzki for **Figure 1**. We thank O. Ayala, B. Devenish, A. Lanotte, and B. Rosa for providing insightful comments on this review.

LITERATURE CITED

Albrecht BA. 1989. Aerosols, cloud microphysics, and fractional cloudiness. *Science* 245:1227–30

Andrejczuk M, Grabowski WW, Malinowski SP, Smolarkiewicz PK. 2004. Numerical simulation of cloud clear air interfacial mixing. *J. Atmos. Sci.* 61:1726–39

Andrejczuk M, Grabowski WW, Malinowski SP, Smolarkiewicz PK. 2006. Numerical simulation of cloud-clear air interfacial mixing: effects on cloud microphysics. *J. Atmos. Sci.* 63:3204–25

Andrejczuk M, Grabowski WW, Malinowski SP, Smolarkiewicz PK. 2009. Numerical simulation of cloud-clear air interfacial mixing: homogeneous versus inhomogeneous mixing. *J. Atmos. Sci.* 66:2493–500

Andrejczuk M, Grabowski WW, Reisner J, Gadian A. 2010. Cloud-aerosol interactions for boundary-layer stratocumulus in the Lagrangian Cloud Model. *J. Geophys. Res.* 115:D22214

Andrejczuk M, Reisner JM, Henson B, Dubey MK, Jeffery CA. 2008. The potential impacts of pollution on a nondrizzling stratus deck: Does aerosol number matter more than type? *J. Geophys. Res.* 113:D19204

Arenberg D. 1939. Turbulence as a major factor in the growth of cloud droplets. *Bull. Am. Meteorol. Soc.* 20:444–45

Ayala O, Grabowski WW, Wang L-P. 2007. A hybrid approach for simulating turbulent collisions of hydrodynamically-interacting particles. *J. Comput. Phys.* 225:51–73

Ayala O, Rosa B, Wang L-P. 2008a. Effects of turbulence on the geometric collision rate of sedimenting droplets: Part 2. Theory and parameterization. *New J. Phys.* 10:075016

Develops the most comprehensive parameterization of turbulent collision kernel for cloud droplets.

Ayala O, Rosa B, Wang L-P, Grabowski WW. 2008b. Effects of turbulence on the geometric collision rate of sedimenting droplets: Part 1. Results from direct numerical simulation. *New J. Phys.* 10:075015. Corrigendum. 10:099802

Beard KV. 1976. Terminal velocity and shape of cloud and precipitation drops aloft. *J. Atmos. Sci.* 33:851–64

Beard KV, Ochs HT. 1993. Warm-rain initiation: an overview of microphysical mechanisms. *J. Appl. Meteorol.* 32:608–25

Bec J, Biferale L, Cencini M, Lanotte AS, Toschi F. 2010. Intermittency in the velocity distribution of heavy particles in turbulence. *J. Fluid Mech.* 646:527–36

Bender FAM, Rodhe H, Charlson RJ, Ekman AML, Loeb N. 2006. 22 views of the global albedo: comparison between 20 GCMs and two satellites. *Tellus A* 58:320–30

Berry EX, Reinhardt RL. 1974. An analysis of cloud drop growth by collection: Part 1. Double distribution. *J. Atmos. Sci.* 31:1814–24

Bony S, Dufresne JL. 2005. Marine boundary layer clouds at the heart of tropical cloud feedback uncertainties in climate models. *Geophys. Res. Lett.* 32:L20806

Brenguier JL. 1993. Observations of cloud microstructure at the centimeter scale. *J. Appl. Meteorol.* 4:783–93

Brenguier JL, Chaumat L. 2001. Droplet spectra broadening in cumulus clouds. Part I: Broadening in adiabatic cores. *J. Atmos. Sci.* 58:628–41

Brenguier JL, Grabowski WW. 1993. Cumulus entrainment and cloud droplet spectra: a numerical model within a two-dimensional dynamical framework. *J. Atmos. Sci.* 50:120–36

Celani A, Falkovich G, Mazzino A, Seminara A. 2005. Droplet condensation in turbulent flows. *Europhys. Lett.* 70:775–81

Celani A, Mazzino A, Seminara A, Tizzi M. 2007. Droplet condensation in two-dimensional Bolgiano turbulence. *J. Turbul.* 8:17

Chaumat L, Brenguier J-L. 2001. Droplet spectra broadening in cumulus clouds. Part II: Microscale droplet concentration heterogeneities. *J. Atmos. Sci.* 58:642–54

Chun J, Koch D, Rani SL, Ahluwalia A, Collins LR. 2005. Clustering of aerosol particles in isotropic turbulence. *J. Fluid Mech.* 536:219–51

Collins LR, Keswani A. 2004. Reynolds number scaling of particle clustering in turbulent aerosols. *New J. Phys.* 6:119

Cooper WA. 1989. Effects of variable droplet growth histories on droplet size distributions. Part I: Theory. *J. Atmos. Sci.* 46:1301–11

Cooper WA, Lasher-Trapp SG, Blyth AM. 2011. Initiation of coalescence in a cumulus cloud: a beneficial influence of entrainment and mixing. *Atmos. Chem. Phys. Discuss.* 11:10557–613

Davila J, Hunt JCR. 2001. Settling of small particles near vortices and in turbulence. *J. Fluid Mech.* 440:117–45

de Almeida FC. 1976. The collisional problem of cloud droplets moving in a turbulent environment—Part I: A method of solution. *J. Atmos. Sci.* 33:1571–78

de Almeida FC. 1979. The collisional problem of cloud droplets moving in a turbulent environment—Part II: Turbulent collision efficiencies. *J. Atmos. Sci.* 36:1564–76

Derevyanko S, Falkovich G, Turitsyn S. 2008. Evolution of non-uniformly seeded warm clouds in idealized turbulent conditions. *New J. Phys.* 10:075019

Provides a thorough review of related work on droplet clustering.

Devenish BJ, Bartello P, Brenguier J-L, Collins LR, Grabowski WW, et al. 2012. Droplet growth in warm turbulent clouds. *Q. J. R. Meteorol. Soc.* 138:1401–129

East TWR, Marshall JS. 1954. Turbulence in clouds as a factor in precipitation. *Q. J. R. Meteorol. Soc.* 80:26–47

Eaton JK, Fessler JR. 1994. Preferential concentration of particles by turbulence. *Int. J. Multiphase Flow* 20:169–209

Falkovich G, Fouxon A, Stepanov MG. 2002. Acceleration of rain initiation by cloud turbulence. *Nature* 419:151–54

Falkovich G, Pumir A. 2007. Sling effect in collisions of water droplets in turbulent clouds. *J. Atmos. Sci.* 64:4497–505

Fiori E, Parodi A, Siccardi F. 2011. Uncertainty in prediction of deep moist convective processes: turbulence parameterizations, microphysics and grid-scale effects. *Atmos. Res.* 100:447–56

Franklin CN. 2008. A warm rain microphysics parameterization that includes the effect of turbulence. *J. Atmos. Sci.* 65:1795–815

Franklin CN, Vaillancourt PA, Yau MK. 2007. Statistics and parameterizations of the effect of turbulence on the geometric collision kernel of cloud droplets. *J. Atmos. Sci.* 64:938–54

Franklin CN, Vaillancourt PA, Yau MK, Bartello P. 2005. Collision rates of cloud droplets in turbulent flow. *J. Atmos. Sci.* 62:2451–66

Gabilly A. 1949. On the role that turbulence can play in the coalescence of cloud droplets. *Ann. Geophys.* 5:232–34

Gao H, Li H, Wang L-P. 2012. Lattice Boltzmann simulation of turbulent flow laden with finite-size particles. *Comp. Math. Appl.* In press. doi: 10.1016/j.camwa.2011.06.028

Gerber H, Arends BG, Ackerman AS. 1994. New microphysics sensor for aircraft use. *Atmos. Res.* 31:235–52

Ghosh S, Davila J, Hunt JCR, Srdic A, Fernando HJS, Jonas P. 2005. How turbulence enhances coalescence of settling particles with applications to rain in clouds. *Proc. R. Soc. A* 461:3059–88

Ghosh S, Jonas PR. 2001. Some analytical calculations on the effect of turbulence on the settling and growth of cloud droplets. *Geophys. Res. Lett.* 28:3883–86

Grabowski WW, Clark TL. 1993. Cloud-environment interface instability, part II: Extension to three spatial dimensions. *J. Atmos. Sci.* 50:555–73

Good GH, Gerashchenko S, Warhaft Z. 2012. Intermitency and inertial particle entrainment at a turbulent interface: the effect of the large-scale eddies. *J. Fluid Mech.* 694:371–98

Grabowski WW, Vaillancourt P. 1999. Comments on preferential concentration of cloud droplets by turbulence: effects on early evolution of cumulus cloud droplet spectra. *J. Atmos. Sci.* 56:1433–36

Presents an impact study of the turbulent collision kernel using a parcel model.

Grabowski WW, Wang LP. 2009. Diffusional and accretional growth of water drops in a rising adiabatic parcel: effects of the turbulent collision kernel. *Atmos. Chem. Phys.* 9:2335–53

Grover SN, Pruppacher HR. 1985. The effect of vertical turbulent fluctuations in the atmosphere on the collection of aerosol particles by cloud drops. *J. Atmos. Sci.* 42:2305–18

Hall WD. 1980. A detailed microphysical model within a two-dimensional dynamic framework: model description and preliminary results. *J. Atmos. Sci.* 37:2486–507

Haman KE, Makulski A, Malinowski SP, Busen R. 1997. A new ultrafast thermometer for airborne measurements in clouds. *J. Atmos. Ocean. Technol.* 14:217–27

Haman KE, Malinowski SP, Kurowski MJ, Gerber H, Brenguier JL. 2007. Small scale mixing processes at the top of a marine stratocumulus: a case study. *Q. J. R. Meteorol. Soc.* 133:213–26

Haman KE, Malinowski SP, Strus BD, Busen R, Stefko A. 2001. Two new types of ultrafast aircraft thermometer. *J. Atmos. Ocean. Technol.* 18:117–34

Hsieh WC, Jonsson H, Wang L-P, Buzorius G, Flagan RC, Seinfeld JH, Nenes A. 2009. On the representation of droplet coalescence and autoconversion: evaluation using ambient cloud droplet size distributions. *J. Geophy. Res.* 114:D07201

Jonas PR. 1996. Turbulence and cloud microphysics. *Atmos. Res.* 40:283–306

Khain AP, Pinsky M. 1997. Turbulence effects on the collision kernel, part 2: increase of swept volume of colliding drops. *Q. J. R. Meteorol. Soc.* 123: 1543–60

Khain AP, Pinsky M, Elperin T, Kleeorin N, Rogachevskii I, Kostinski A. 2007. Critical comments to results of investigations of drop collisions in turbulent clouds. *Atmos. Res.* 86:1–20

Klett JD, Davis MH. 1973. Theoretical collision efficiencies of cloud droplets at small Reynolds numbers. *J. Atmos. Sci.* 30:107–17

Kostinski AB, Shaw RA. 2001. Scale-dependent droplet clustering in turbulent clouds. *J. Fluid Mech.* 434:389–98

Koziol AS, Leighton HG. 1996. The effect of turbulence on the collision rates of small cloud drops. *J. Atmos. Sci.* 53:1910–20

Lanotte AS, Seminara A, Toschi F. 2009. Cloud droplet growth by condensation in homogeneous isotropic turbulence. *J. Atmos. Sci.* 66:1685–97

Lasher-Trapp SG, Cooper WA, Blyth AM. 2005. Broadening of droplet size distributions from entrainment and mixing in a cumulus cloud. *Q. J. R. Meteorol. Soc.* 131:195–220

Lau KM, Wu H-T. 2003. Warm rain processes over tropical oceans and climate implications. *Geophys. Res. Lett.* 30:2290

Lehmann K, Siebert H, Shaw RA. 2009. Homogeneous and inhomogenous mixing in cumulus clouds: dependence on local turbulence structure. *J. Atmos. Sci.* 66:3641–59

Long AB. 1974. Solutions to the droplet coalescence equation for polynomial kernels. *J. Atmos. Sci.* 11:1040–52

Lu J, Nordsiek H, Shaw RA. 2010. Clustering of settling charged particles in turbulence: theory and experiments. *New J. Phys.* 12:123030

MacPherson JI, Isaac GA. 1977. Turbulent characteristics of some Canadian cumulus clouds. *J. Appl. Meteorol.* 16:81–90

Malinowski SP, Andrejczuk M, Grabowski WW, Korczyk P, Kowalewski TA, Smolarkiewicz PK. 2008. Laboratory and modeling studies of cloud-clear air interfacial mixing: anisotropy of small-scale turbulence due to evaporative cooling. *New J. Phys.* 10:075020

Maxey MR. 1987. The gravitational settling of aerosol-particles in homogeneous turbulence and random flow fields. *J. Fluid Mech.* 174:441–65

Meneveau C, Sreenivasan KR. 1991. The multifractal nature of turbulent energy dissipation. *J. Fluid Mech.* 224:429–84

Montgomery RB. 1947. Viscosity and thermal conductivity of air and diffusivity of water vapor in air. *J. Atmos. Sci.* 6:193–96

Onishi R, Takahashi K, Komori S. 2009. Influence of gravity on collisions of monodispersed droplets in homogeneous isotropic turbulence. *Phys. Fluids* 21:125108

Paoli R, Shariff K. 2009. Turbulent condensation of droplets: direct simulation and a stochastic model. *J. Atmos. Sci.* 66:723–40

Pincus R, Baker MB. 1994. Effect of precipitation on the albedo susceptibility of clouds in the marine boundary layer. *Nature* 372:250–52

Pinsky MB, Khain AP. 1997. Formation of inhomogeneity in drop concentration induced by the inertia of drops falling in a turbulent flow, and the influence of the inhomogeneity on the drop-spectrum broadening. *Q. J. R. Meteorol. Soc.* 123:165–86

Pinsky MB, Khain AP. 2002. Effects of in-cloud nucleation and turbulence on droplet spectrum formation in cumulus clouds. *Q. J. R. Meteorol. Soc.* 128:501–33

Pinsky M, Khain A. 2003. Fine structure of cloud droplet concentration as seen from the Fast-FSSP measurements. Part II: Results of in situ observations. *J. Appl. Meteorol.* 42:65–73

Pinsky MB, Khain AP. 2004. Collisions of small drops in a turbulent flow. Part II: Effects of flow accelerations. *J. Atmos. Sci.* 61:1926–39

Pinsky MB, Khain AP, Grits B, Shapiro M. 2006. Collisions of small drops in a turbulent flow. Part III: Relative droplet fluxes and swept volumes. *J. Atmos. Sci.* 63:2123–39

Pinsky M, Khain AP, Krugliak H. 2008. Collisions of cloud droplets in a turbulent flow. Part V: Application of detailed tables of turbulent collision rate enhancement to simulation of droplet spectra evolution. *J. Atmos. Sci.* 65: 357–74

Pinsky MB, Khain AP, Levin Z. 1999a. The role of the inertia of cloud drops in the evolution of the spectra during drop growth by diffusion. *Q. J. R. Meteorol. Soc.* 125:553–81

Pinsky MB, Khain AP, Shapiro M. 1999b. Collisions of small drops in a turbulent flow. Part I: Collision efficiency. Problem formulation and preliminary results. *J. Atmos. Sci.* 56:2585–600

Pinsky MB, Khain AP, Shapiro M. 2001. Collision efficiency of drops in a wide range of Reynolds numbers: Effects of pressure on spectrum evolution. *J. Atmos. Sci.* 58:742–64

Pinsky MB, Khain AP, Shapiro M. 2007. Collisions of cloud droplets in a turbulent flow. Part IV: droplet hydrodynamic interaction. *J. Atmos. Sci.* 64:2462–82

Pinsky M, Shapiro M, Khain A, Wirzberger H. 2004. A statistical model of strains in homogeneous and isotropic turbulence. *Physica D* 191:297–313

Politovich MK, Cooper WA. 1988. Variability of supersaturation in cumulus clouds. *J. Atmos. Sci.* 45:1651–64

Pruppacher HR, Klett JD. 1997. *Microphysics of Clouds and Precipitation*. Dordrecht: Kluwer Acad. 954 pp.

Raes F. 2006. Take a glass of water: concepts from physical chemistry used in describing the behaviour of aerosol and cloud droplets. *J. Phys. IV* 139:63–80

Reuter GW, De Villiers R, Yavin Y. 1988. The collection kernel for two falling cloud drops subjected to random perturbations at a turbulent airflow: a sthocastic model. *J. Atmos. Sci.* 45:765–73

Riemer N, Wexler AS. 2005. Droplets to drops by turbulent coagulation. *J. Atmos. Sci.* 62:1962–75

Rogers RR, Yau MK. 1989. *A Short Course in Cloud Physics*. Burlington, MA: Butterworth-Heinemann. 298 pp.

Rosa B, Bajer K, Haman KE, Szoplik T. 2005. Theoretical and experimental characterization of the ultrafast aircraft thermometer: reduction of aerodynamic disturbances and signal processing. *J. Atmos. Ocean. Technol.* 22:988–1003

Rosa B, Parishani H, Ayala O, Wang L-P, Grabowski WW. 2011a. Kinematic and dynamic pair collision statistics of sedimenting inertial particles relevant to warm rain initiation. *J. Phys. Conf. Ser.* 318:072016

Rosa B, Wang L-P, Maxey MR, Grabowski WW. 2011b. An accurate model for aerodynamic interactions of cloud droplets. *J. Comput. Phys.* 230:8109–33

Saffman PG, Turner JS. 1956. On the collision of drops in turbulent clouds. *J. Fluid Mech.* 1:16–30

Salazar JPLC, de Jong J, Cao L, Woodward SH, Meng H, Collins LR. 2008. Experimental and numerical investigation of inertial particle clustering in isotropic turbulence. *J. Fluid Mech.* 600:245–56

Seifert A, Nuijens L, Stevens B. 2010. Turbulence effects on warm-rain autoconversion in precipitating shallow convection. *Q. J. R. Meteorol. Soc.* 136:1753–62

Shaw RA. 2000. Supersaturation intermittency in turbulent clouds. *J. Atmos. Sci.* 57:3452–56

Shaw RA. 2003. Particle-turbulence interactions in atmospheric clouds. *Annu. Rev. Fluid Mech.* 35:183–227

Presents a wonderful review of cloud turbulence and open cloud microphysics questions.

Shaw RA, Oncley SP. 2001. Acceleration intermittency and enhanced collision kernels in turbulent clouds. *Atmos. Res.* 59–60:77–87

Shaw RA, Reade WC, Collins LR, Verlinde J. 1998. Preferential concentration of clouds droplets by turbulence: effects on early evolution of cumulus cloud droplet spectra. *J. Atmos. Sci.* 55:1965–76

Shima S, Kusano K, Kawano A, Sugiyama T, Kawahara S. 2009. The super-droplet method for the numerical simulation of clouds and precipitation: a particle-based and probabilistic microphysics model coupled with a non-hydrostatic model. *Q. J. R. Meteorol. Soc.* 135:1307–20

Sidin RSR, Ijzermans RHA, Reeks MW. 2009. A Lagrangian approach to droplet condensation in atmospheric clouds. *Phys. Fluids* 21:106603

Siebert H, Lehmann K, Shaw RA. 2007. On the use of hot-wire anemometers for turbulence measurements in clouds. *J. Atmos. Ocean. Technol.* 24:980–93

Siebert H, Lehmann K, Wendisch M. 2006a. Observations of small-scale turbulence and energy dissipation rates in the cloudy boundary layer. *J. Atmos. Sci.* 61:1451–66

Siebert H, Lehmann K, Wendisch M, Franke H, Maser R, et al. 2006b. Probing finescale dynamics and microphysics of clouds with helicopter-borne measurements. *Bull. Am. Meteorol. Soc.* 87:1727–38

Presents an overview of the design and capability of ACTOS.

Siebert H, Shaw RA, Warhaft Z. 2010. Statistics of small-scale velocity fluctuations and internal intermittency in marine stratocumulus clouds. *J. Atmos. Sci.* 67:262–73

Siebesma AP, Bretherton CS, Brown A, Chlond A, Cuxart J, et al. 2003. A large eddy simulation intercomparison study of shallow cumulus convection. *J. Atmos. Sci.* 60:1201–19

Slawinska J, Grabowski WW, Pawlowska H, Morrison H. 2012. Droplet activation and mixing in large-eddy simulation of a shallow cumulus field. *J. Atmos. Sci.* 69:444–62

Slingo A. 1990. Sensitivity of the Earth's radiation budget to changes in low clouds. *Nature* 343:49–51

Spyksma K, Bartello P. 2008. Small-scale moist turbulence in numerically generated convective clouds. *J. Atmos. Sci.* 65:1967–78
Squires KD, Eaton JK. 1990. Particle response and turbulence modification in isotropic turbulence. *Phys. Fluids A* 2:1191–203
Squires P. 1952. The growth of cloud drops by condensation. 1. General characteristics. *Aust. J. Sci. Res. A* 5:59–86
Srivastava RC. 1989. Growth of cloud drops by condensation: a criticism of currently accepted theory and a new approach. *J. Atmos. Sci.* 46:869–87
Sundaram S, Collins LR. 1997. Collision statistics in an isotropic, particle-laden turbulent suspension. *J. Fluid Mech.* 335:75–109
Tennekes H, Woods JD. 1973. Coalescence in a weakly turbulent cloud. *Q. J. R. Meteorol. Soc.* 99:758–63
Twomey S. 1974. Pollution and the planetary albedo. *Atmos. Environ.* 8:1251–56
Twomey S. 1977. The influence of pollution on the shortwave albedo of clouds. *J. Atmos. Sci.* 34:1149–52
Vaillancourt PA, Yau MK. 2000. Review of particle-turbulence interactions and consequences for cloud physics. *Bull. Am. Meteorol. Soc.* 81:285–98
Vaillancourt PA, Yau MK, Bartello P, Grabowski WW. 2002. Microscopic approach to cloud droplet growth by condensation. Part II: Turbulence, clustering, and condensational growth. *J. Atmos. Sci.* 59:3421–35
Vaillancourt PA, Yau MK, Grabowski WW. 2001. Microscopic approach to cloud droplet growth by condensation. Part I: Model description and results without turbulence. *J. Atmos. Sci.* 58:1945–64
Wang L-P, Ayala O, Grabowski WW. 2007a. Effects of aerodynamic interactions on the motion of heavy particles in a bidisperse suspension. *J. Turbul.* 8:N25
Wang L-P, Ayala O, Kasprzak SE, Grabowski WW. 2005. Theoretical formulation of collision rate and collision efficiency of hydrodynamically-interacting cloud droplets in turbulent atmosphere. *J. Atmos. Sci.* 62:2433–50
Wang L-P, Ayala O, Parishani H, Grabowski WW, Wyszogrodzki AA, et al. 2011. Towards an integrated multiscale simulation of turbulent clouds on PetaScale computers. *J. Phys. Conf. Ser.* 318:072021
Wang L-P, Ayala O, Rosa B, Grabowski WW. 2008. Turbulent collision efficiency of heavy particles relevant to cloud droplets. *New J. Phys.* 10:075013
Wang L-P, Ayala O, Xue Y, Grabowski WW. 2006a. Comments on "Droplets to drops by turbulent coagulation." *J. Atmos. Sci.* 63:2397–401
Wang L-P, Franklin CN, Ayala O, Grabowski WW. 2006b. Probability distributions of angle of approach and relative velocity for colliding droplets in a turbulent flow. *J. Atmos. Sci.* 63:881–900
Wang L-P, Grabowski WW. 2009. The role of air turbulence in warm rain initiation. *Atmos. Sci. Lett.* 10:1–8
Wang L-P, Maxey MR. 1993. Settling velocity and concentration distribution of heavy particles in homogeneous isotropic turbulence. *J. Fluid Mech.* 256:27–68
Wang L-P, Rosa B, Gao H, He G-W, Jin G-D. 2009. Turbulent collision of inertial particles: point-particle based, hybrid simulations and beyond. *Int. J. Multiphase Flow* 35:854–67
Wang L-P, Wexler AS, Zhou Y. 1998. Statistical mechanical descriptions of turbulent coagulation. *Phys. Fluids* 10:2647–51
Wang L-P, Wexler AS, Zhou Y. 2000. Statistical mechanical descriptions of turbulent coagulation of inertial particles. *J. Fluid Mech.* 415:117–53
Wang L-P, Xue Y, Grabowski WW. 2007b. A bin integral method for solving the kinetic collection equation. *J. Comput. Phys.* 225:51–73
Warhaft Z. 2009. Laboratory studies of droplets in turbulence: towards understanding the formation of clouds. *Fluid Dyn. Res.* 41:011201
Warner J. 1955. The water content of cumuliform cloud. *Tellus* 7:449–57
Wilkinson M, Mehlig B, Bezuglyy V. 2006. Caustic activation of rain showers. *Phys. Rev. Lett.* 97:048501
Woittiez EJP, Jonker HJJ, Portela LM. 2009. On the combined effects of turbulence and gravity on droplet collisions in clouds: a numerical study. *J. Atmos. Sci.* 66:1926–43
Xue Y, Wang L-P, Grabowski WW. 2008. Growth of cloud droplets by turbulent collision-coalescence. *J. Atmos. Sci.* 65:331–56

Presents the first DNS study of the turbulent diffusional growth of cloud droplets.

Introduces hybrid DNS to study turbulent collision efficiency.

Provides scaling arguments for enhancement of the collision kernel by air turbulence.

Zaichik LI, Alipchenkov VM. 2003. Pair dispersion and preferential concentration of particles in isotropic turbulence. *Phys. Fluids.* 15:1776–87

Zaichik LI, Simonin O, Alipchenkov VM. 2003. Two statistical models for predicting collision rates of inertial particles in homogeneous isotropic turbulence. *Phys. Fluids* 15:2995–3005

Zaichik LI, Simonin O, Alipchenkov VM. 2006. Collision rates of bidisperse inertial particles in isotropic turbulence. *Phys. Fluids* 18:035110

Zhou Y, Wexler AS, Wang LP. 2001. Modelling turbulent collision of bidisperse inertial particles. *J. Fluid Mech.* 433:77–104

Annual Review of
Fluid Mechanics

Volume 45, 2013

Contents

Hans W. Liepmann, 1914–2009
Roddam Narasimha, Anatol Roshko, and Morteza Gharib 1

Philip G. Saffman
D.I. Pullin and D.I. Meiron 19

Available Potential Energy and Exergy in Stratified Fluids
Rémi Tailleux 35

The Fluid Dynamics of Tornadoes
Richard Rotunno 59

Nonstandard Inkjets
Osman A. Basaran, Haijing Gao, and Pradeep P. Bhat 85

Breaking Waves in Deep and Intermediate Waters
Marc Perlin, Wooyoung Choi, and Zhigang Tian 115

Balance and Spontaneous Wave Generation in Geophysical Flows
J. Vanneste 147

Wave Packets and Turbulent Jet Noise
Peter Jordan and Tim Colonius 173

Leidenfrost Dynamics
David Quéré 197

Ice-Sheet Dynamics
Christian Schoof and Ian Hewitt 217

Flow in Foams and Flowing Foams
Sylvie Cohen-Addad, Reinhard Höhler, and Olivier Pitois 241

Moving Contact Lines: Scales, Regimes, and Dynamical Transitions
Jacco H. Snoeijer and Bruno Andreotti 269

Growth of Cloud Droplets in a Turbulent Environment
Wojciech W. Grabowski and Lian-Ping Wang 293

The Fluid Mechanics of Cancer and Its Therapy
Petros Koumoutsakos, Igor Pivkin, and Florian Milde 325

Analysis of Fluid Flows via Spectral Properties of the Koopman Operator
Igor Mezić 357

The Interaction of Jets with Crossflow
Krishnan Mahesh 379

Particle Image Velocimetry for Complex and Turbulent Flows
Jerry Westerweel, Gerrit E. Elsinga, and Ronald J. Adrian 409

Fluid Dynamics of Human Phonation and Speech
Rajat Mittal, Byron D. Erath, and Michael W. Plesniak 437

Sand Ripples and Dunes
François Charru, Bruno Andreotti, and Philippe Claudin 469

The Turbulent Flows of Supercritical Fluids with Heat Transfer
Jung Yul Yoo 495

Indexes

Cumulative Index of Contributing Authors, Volumes 1–45 527

Cumulative Index of Chapter Titles, Volumes 1–45 536

Errata

An online log of corrections to *Annual Review of Fluid Mechanics* articles may be found at http://fluid.annualreviews.org/errata.shtml